SINGLE-MOLECULE MASS SPECTROMETRY

David Z. Keifer and Martin F. Jarrold*
Department of Chemistry, Indiana University, 800 E. Kirkwood Ave., Bloomington, IN 47401

Received 2 December 2015; accepted 15 January 2016

Published online in Wiley Online Library (wileyonlinelibrary.com). DOI 10.1002/mas.21495

In single-molecule mass spectrometry, the mass of each ion is measured individually; making it suitable for the analysis of very large, heterogeneous objects that cannot be analyzed by conventional means. A range of single-molecule mass spectrometry techniques has been developed, including time-of-flight with cryogenic detectors, a quadrupole ion trap with optical detection, single-molecule Fourier transform ion cyclotron resonance, charge detection mass spectrometry, quadrupole ion traps coupled to charge detector plates, and nanomechanical oscillators. In addition to providing information on mass and heterogeneity, these techniques have been used to study impact craters from cosmic dust, monitor the assembly of viruses, elucidate the fluorescence dynamics of quantum dots, and much more. This review focuses on the merits of each of these technologies, their limitations, and their applications. © 2016 Wiley Periodicals, Inc. Mass Spec Rev

Keywords: *single-molecule; charge detection; optical detection; cryogenic detector; nanomechanical resonator; nanomechanical oscillator; quadrupole ion trap; time of flight mass spectrometry; Fourier transform ion cyclotron resonance; electrostatic ion trap; cone trap*

I. INTRODUCTION

The *m*/*z* (mass to charge ratio) spectrum for a small protein ionized by electrospray contains a series of peaks from different charge states. The separation between the peaks can be used to deduce the charge, which combined with the *m*/*z* gives the mass. Native mass spectrometry (electrospray from non-denaturing solutions) (Chowdhury, Katta, & Chait, 1990; Ganem, Li, & Henion, 1991; Loo, 1997; van den Heuvel & Heck, 2004; Zhou & Robinson, 2010) allows large assemblies to be placed into the gas phase. As size increases, it becomes increasingly difficult to resolve the charge states. Heck and co-workers have provided a convincing argument that this loss of resolution is not instrumental, but results from heterogeneity (Lössl, Snijder, & Heck, 2014).

There are two types of heterogeneity, intrinsic and extrinsic. By extrinsic, we mean objects that have a single well-defined mass, but they appear heterogeneous because their ions are incompletely desolvated, possess different numbers or types of counter ions, or form adducts with impurities in solution. In this case, a resolved *m*/*z* spectrum may be generated with extensive purification of the sample, and through collisional activation to remove adducts, counter ions, and any remaining solvent. GroEL, an 800 kDa protein complex, is an example of extrinsic heterogeneity. Well-resolved *m*/*z* spectra can be obtained, but only after a substantial effort to purify the sample.

For some objects, purification does not result in a resolved *m*/*z* spectrum. In these cases, the ions might be intrinsically heterogeneous, which means that the objects themselves do not have a single, well-defined mass. Cells, polymers, nanoparticles, and aerosols are examples. In general, larger objects are more likely to be intrinsically heterogeneous. Intrinsically heterogeneous objects are also likely to be extrinsically heterogeneous, further congesting the *m*/*z* spectrum. If the number of masses present is much less than the number of ions sampled then, in principle, the charge states could be resolved if the resolving power is sufficiently high. However, the charge states cannot be resolved if the number of masses present is much greater than the number of ions sampled. At some point, charge-state resolution will be lost (Wong, Meng, & Fenn, 1988; Stockley et al., 2007; Bereszczak et al., 2014).

One solution to this problem is to perform a single-molecule mass measurement where the mass of each individual ion is determined. If measurements were performed for a large number of ions, then a mass distribution can be constructed by binning them into a histogram. The width of the distribution can provide valuable information about sample heterogeneity and its origin. In addition, some of the techniques used to perform single-molecule mass measurements also provide the opportunity to trap an ion for a long time and investigate its properties. These studies can provide valuable information about how the properties differ from the ensemble average.

Single-molecule mass spectrometry (MS) is not limited by charge-state resolution, so it can be extended to arbitrarily high masses and broad heterogeneity. A single-molecule mass measurement can be accomplished in several ways. Some techniques involve simultaneous measurement of *m*/*z* and charge, including direct charge detection in Fourier transform ion cyclotron resonance (FTICR), charge detection mass spectrometry (CDMS), and a quadrupole ion trap (QIT) with a charge detecting plate. Time-of-flight MS (TOFMS) with cryogenic detectors can potentially measure *m*/*z* and charge simultaneously, but the method currently does not perform well for large, highly-charged ions. Other techniques involve charge stepping, where the *m*/*z* of a single ion is measured for several different values of charge to deduce mass. Charge stepping can be performed in an FTICR or in a QIT with optical detection. Finally, mass can be measured independently of charge with a nanomechanical oscillator, where the resonant frequency of the device changes as mass accretes on it. This review will focus on the advantages and disadvantages of single-molecule MS techniques. Applications will be noted along the way.

Contract grant sponsor: National Science Foundation; Contract grant number: CHE–1531823.

Correspondence to: Martin F. Jarrold, Department of Chemistry, Indiana University, 800 E. Kirkwood Ave., Bloomington, IN 47401. E-mail: mfj@indiana.edu

We would be remiss if we did not recognize the progress that has been made in studying high-mass ions with conventional MS. There are several technical issues in addition to the problem of heterogeneity and charge-state resolution. The low detection efficiency of electron multipliers for large ions is well known (Gilmore & Seah, 2000; Westmacott et al., 2000; Fraser, 2002). For mass spectrometers that use image charge detection such as FTICR and the orbitrap, the finite charge capacity (Marshall, Hendrickson, & Jackson, 1998; Hu, Cooks, & Noll, 2007) of the cell can preclude analysis of a representative ensemble for a heterogeneous sample. Recent modifications to the orbitrap have extended its mass range to ~1 megadalton (MDa) with substantially better resolving power than TOF (Rose et al., 2012; Dyachenko et al., 2015).

Small viruses have masses of a few MDa and they have become attractive targets for high-mass studies. Robinson and co-workers were the first to measure the mass of a virus capsid with conventional MS. An m/z spectrum with barely resolved charge states was measured for the 2.5 MDa MS2 capsid with TOFMS (Tito et al., 2000). At the time, this was the largest mass measured with conventional MS. Within the last decade, Heck and co-workers have obtained well-resolved m/z spectra for hepatitis B virus (HBV) capsids formed from the assembly domain of the capsid protein (Cp149) (Uetrecht et al., 2008a,b, 2010). The HBV Cp149 $T = 3$ capsid (with 180 capsid proteins) has a mass just over 3 MDa, and the $T = 4$ (with 240 capsid proteins) has a mass just over 4 MDa. Charge state resolution was lost for capsids assembled from the full length capsid protein (HBV Cp183). This loss was attributed to the retention of short RNA fragments by the binding domain (Uetrecht et al., 2008a). The same group has published m/z spectra with incipient charge-state resolution for the Prohead I form of HK97 bacteriophage capsids weighing ~18 MDa (Snijder et al., 2013). This remarkable achievement represents the highest mass measured so far with conventional MS. They estimated the upper mass limit of conventional electrospray MS to be ~20 MDa because of extrinsic heterogeneity from water and salt adducts. Except in rare cases (Snijder et al., 2014), conventional MS requires strict homogeneity to weigh ions in the MDa range. It is no coincidence that all of the examples mentioned above are virus capsids. Icosahedral virus capsids that have been studied by MS are composed of a specific number of (usually) identical proteins, and are therefore much less heterogeneous than other complexes of similar size.

There have been several recent reviews of high-mass MS, but they have focused primarily on conventional MS, with only some attention paid to single-molecule MS (Peng, Chou, & Patil, 2014; Snijder & Heck, 2014). Chang reviewed single-molecule MS in 2009 (Chang, 2009), but much progress has been made since then.

Finally, a ground rule; in an ensemble measurement, the precision is represented by the resolution or resolving power. When masses are measured individually, the precision can be determined by measuring the masses of many identical objects or the same object multiple times. Binning the results into a histogram should lead to a Gaussian peak shape with a full width at half maximum (FWHM) 2.3548 times the root mean square deviation (RMSD). In what follows, we use the resolving power ($m/\Delta m$ FWHM) to compare the precision of the different techniques discussed here.

II. CRYOGENIC DETECTORS

TOFMS has, in theory, an unlimited m/z range. It is often coupled with MALDI (matrix-assisted laser-desorption ionization). MALDI produces much lower charge states than electrospray, which can lead to large m/z values. Microchannel plates (MCPs), the detectors most commonly used with TOFMS, have poor detection efficiency for high-m/z ions (Gilmore & Seah, 2000; Westmacott et al., 2000; Fraser, 2002). MCPs also cannot distinguish between different species with the same m/z, such as singly charged monomers and doubly charged dimers. A variety of solutions to the high-m/z detection efficiency problem have been developed: conversion dynodes (Spengler et al., 1990; Weidmann & Zenobi, 2014), ion-to-photon detectors (Dubois, Knochenmuss, & Zenobi, 1999; Gilmore & Seah, 2000; Li et al., 2007), nanomembrane oscillators (Park et al., 2011, 2013), and cryogenic detectors, including microcalorimeters (Hilton et al., 1998; Frank et al., 1999; Rabin, Hilton, & Martinis, 2001b), superconducting tunneling junctions (STJs) (Twerenbold et al., 1996; Benner et al., 1997), and superconducting stripline detectors (SSLDs) (Koji et al., 2008; Suzuki et al., 2008; Casaburi et al., 2012). Microcalorimeters and STJs are considered in more depth below because they can also measure the charge for individual ions, and hence they can perform single-molecule mass measurements.

Twerenbold was the first to propose the use of a cryogenic detector for high-m/z ions (Twerenbold, 1996). Unlike MCPs that respond to an ion's velocity, cryogenic detectors respond to its kinetic energy. Because all ions of the same charge have the same kinetic energy from acceleration through a fixed potential difference, the detection efficiency should not depend on the m/z. Another advantage of cryogenic detectors is that they can be used to detect neutral molecules from post-source decay (PSD) (Ohkubo et al., 2006), electron-transfer dissociation (ETD), and collisionally activated dissociation (CAD) (Ohkubo et al., 2011; Novotný et al., 2015). The disadvantages of cryogenic detectors are that they require cooling to <4 K and their active area is small ($10^{-4} - 10^{-3}$ cm^2). Microcalorimeters and STJs are also slow, with response times much longer than the sub-nanosecond response time of MCPs. Much work has been done to mitigate these disadvantages (Suzuki et al., 2008; Casaburi et al., 2009, 2012; Zen et al., 2012).

A. Microcalorimeters

A microcalorimeter consists of a metal absorber on an insulating substrate held at <1 K. When an ion strikes the absorber, it deposits its kinetic energy and heats the metal. The temperature shows a sharp rise followed by a slower exponential decay as the heat is dissipated into the substrate. The temperature rise can be measured with very precise thermometers, most commonly by NIS (normal insulator superconductor) tunnel junctions or transition-edge sensors (Frank et al., 1999). Microcalorimeters require extremely low temperatures and precise temperature stabilization. Both of these requirements can be met with a liquid-helium cryostat with an adiabatic demagnetization refrigerator (Hilton et al., 1998).

Ideally, the temperature increase is proportional to the kinetic energy of the impinging ion. However, for polyatomic ions some of the kinetic energy is not deposited into the metal due to internal excitation and possibly fragmentation of the ion.

Twerenbold and co-workers found that singly charged, 66 kDa bovine serum albumin (BSA) ions accelerated to 20 keV deposited on average 11.8 keV, and the distribution was 1.7 keV wide (FWHM) (Hilton et al., 1998). The energy resolving power ($E/\Delta E$ ~7) is sufficient to completely separate singly charged monomers from doubly charged dimers of BSA. However, the fraction of energy deposited depends on the analyte. Whereas BSA deposited ~60% of its energy, lighter sinapinic acid deposited over 70%. The signal decay time constant (due to dissipation of heat into the substrate) is long and ranged from just over ten microseconds to milliseconds (Hilton et al., 1998; Zen et al., 2012); therefore, pulses can pile up if ion fluxes are not kept small.

Singly and doubly charged ions can be completely separated with a microcalorimeter detector, but electrospray generates much more highly charged ions than MALDI. Martinis and co-workers have used a magnetic sector MS with a microcalorimeter detector to measure electrosprayed BSA ions with charge states from +15 to +21 (Rabin, Hilton, & Martinis, 2001b). They found that the pulse height was proportional to $z^{0.4}$ rather than the expected linear dependence. There was insufficient energy resolution to determine charge. Later work by the same group suggested that the sub-linear response was not due to the detector, but rather to the fraction of kinetic energy deposited by the ions (Rabin, Hilton, & Martinis, 2001a).

Cryogenic detectors can be used for single-molecule MS on ions as small as protons (Novotný et al., 2015). These detectors can also be used to detect neutral molecules in tandem MS experiments. Novotný et al. (2015) used a microcalorimeter to study the fragmentation pathways of CH_3^+ and acetone ions. In these experiments, the precursor ions had a known kinetic energy from their acceleration potential, and the kinetic energies of fragments (including neutral fragments) were proportional to their masses. The ability to detect neutral fragments directly, rather than through re-ionization, is a great advantage of using cryogenic detectors in tandem MS experiments, at least for small molecules.

B. Superconducting Tunnel Junctions

An STJ consists of two thin superconducting layers separated by a thin insulating layer. The detector is held at ~10% of the critical superconducting temperature, typically ~1 K or less. When a high-energy ion impinges on one of the superconducting layers, millions of Cooper pairs are broken, and a bias between the two layers causes the liberated electrons to form a tunneling current between them. The first STJ used for TOFMS had a pulse decay time under 10 μs (Twerenbold et al., 1996), somewhat faster than the best microcalorimeters. Newer STJs have decay times on the order of hundreds of nanoseconds (Wenzel et al., 2005). STJs also do not require temperatures as precisely controlled as microcalorimeters. Consequently, STJ detectors have been more widely used in TOFMS than microcalorimeters.

As with the microcalorimeter, the energy deposited into the STJ should be proportional to the ion energy which makes it possible, in principle, to measure the charge. Measuring the charge with an STJ was first explored by Frank and co-workers in 1996 (Frank et al., 1996). For singly charged, 66 kDa human serum albumin ions, the energy resolving power was only ~1.67. Singly and doubly charged ions at the same m/z were not resolved. On the other hand, the energy resolving power for 6 keV X-rays was 20. The higher resolving power with X-rays suggests that the poorer resolving power for macromolecular ions is at least partly due to internal excitation or fragmentation on impact. Similar results were obtained in 1997 by Benner et al. (1997).

Like microcalorimeters, STJs can also be used to detect neutral molecules. In 2006, Ohkubo et al. (2006) detected neutral and ionic PSD fragments of 200 kDa polystyrene and BSA ionized with MALDI. Ohkubo et al. (2011) have also performed tandem MS measurements on acetyl and acetone ions with an STJ, albeit with worse energy resolution than Novotný et al. (2015) managed a few years later. The ability to detect neutral fragments gave them deeper insight into fragmentation pathways than is attainable from conventional MS experiments.

One disadvantage of cryogenic detectors is their small size. This disadvantage can be mitigated with an array. Friedrich et al. (2014) have developed a 112-pixel array of STJs, though this array has not been used for MS. In 2005, Zenobi and co-workers reported results for a 4 × 4 array of STJs developed for MS by Comet AG. Each array element had its own electronics (Wenzel et al., 2005). The total active area was 0.002 cm^2. An array of detectors is preferable to one large detector for several reasons. A single, large detector has higher noise, decreased sensitivity, increased response times, and a higher likelihood of pulse pileup (Frank et al., 1999). Figure 1 shows the m/z spectrum and the scatter plot of deposited energy versus TOF for IgG antibodies measured with the 4 × 4 STJ array (Wenzel et al., 2005). Arrows connect several charge state peaks in the IgG m/z spectrum to their associated bands in the scatter plot. The energy resolution was good enough to distinguish charges for these relatively low charge states. In such cases, cryogenic detectors can be used to

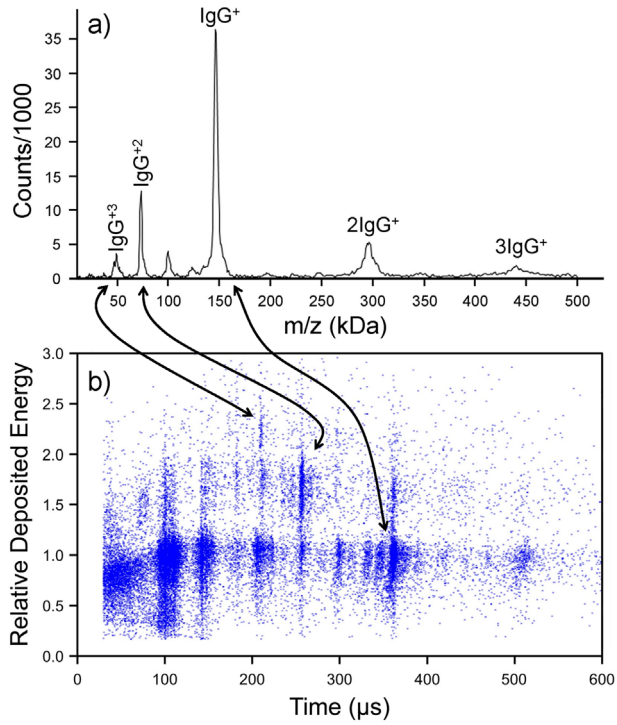

FIGURE 1. (**a**) m/z spectrum of IgG antibodies measured with a 4 × 4 array of STJs. (**b**) Deposited energy versus TOF scatter plot of ions in part a. Adapted from Wenzel et al. (2005).

analyze very heterogeneous analytes, such as ferritin (Plath et al., 2015). Unfortunately, the relationship between the pulse height (i.e., the energy deposited) and ion charge was sub-linear (see Fig. 1b), which was attributed to self-recombination of the electrons into Cooper pairs (Wenzel et al., 2005). The sub-linear response and poor energy resolution has limited the utility of the charge measurement for more massive ions (Aksenov & Bier, 2008). Recent work has focused on improving the energy resolution. In one example, a metal mesh was placed in front of the STJ to block infrared radiation (Shiki et al., 2008) and lower the noise. The energy resolution for argon ions improved by a factor of 2.5. However, the energy resolution for macromolecular ions is not expected to improve by as much because, in this case, the resolution is mainly limited by the energy deposition.

The main benefit of cryogenic detectors is the improved detection efficiency for high-m/z ions, particularly for MALDI TOF. Bier and co-workers have analyzed the ~18 MDa Prohead I form of bacteriophage HK97 with a 16-channel STJ detector. The m/z resolving power was ~15 for the +6 charge state (Plath et al., 2015). As with other STJ TOF studies, there was a sub-linear relationship between the pulse height and the charge state (which extended to above +30). The ion's initial internal energy may be a factor in the sublinear dependence: the internal energy calculated by classical statistical mechanics for an HK97 particle at room temperature is over 180 keV. Because of the difficulties with the charge measurement, TOFMS with a cryogenic detector is usually not the best method for mass analysis of extremely large ions, particularly those generated by electrospray, which produces ions in high charge states.

III. OPTICAL DETECTION WITH A QUADRUPOLE ION TRAP

In 1959, Wuerker, Shelton, & Langmuir (1959) demonstrated that charged iron and aluminum particles, up to 20 μm in diameter, could be trapped in a 3D QIT. Large particles driven by a low-amplitude waveform on the ring electrode will oscillate in relatively slow, Lissajous-like trajectories with small superimposed "micromotions" at the driving frequency. For μm-sized particles of interest here, the frequency is in the radio or audio range. The particles are large enough that their scattered light can be observed visually with a microscope through holes drilled through the ring electrode and end caps. Figure 2a is photograph of a particle's motion observed through a hole in the ring electrode.

To trap individual, charged particles in a QIT and detect their scattered light is one of the most precise ways to measure their m/z. Because the scattered light intensity increases with d^6, where d is particle diameter, this technique is most suitable for particles larger than 50 nm (Nie et al., 2006), so analysis is precluded for many large biologically-important species such as protein complexes, ribosomes, and many viruses. The lower size limit can be overcome by the study of intrinsically (Bell et al., 2014) or tagged (Cai et al., 2002b; Cai, Peng, & Chang, 2003) fluorescent particles, or by the use of a bright probe particle to infer the behavior of a small dark particle (Howder et al., 2015a). However, all these methods have limited applicability.

A. Measurement of Single-Molecule Mass in a QIT

In the work of Wuerker, Shelton, & Langmuir (1959) mentioned above, the m/z of each particle was measured by applying a small AC signal to the end caps and determining the frequency where the particle's secular motion was in resonance with the signal. At that point, the m/z was calculated from the voltages and frequencies applied to the QIT. The mass, however, cannot be determined from a single m/z measurement.

Micron-sized metal particles are so massive that gravity forces them to orbit significantly below the center of the trap. A DC bias can be applied between the top and bottom electrodes (the end caps) to offset the force due to gravity. That voltage provides a second way to measure the m/z of the ion. In 1983, Arnold and co-workers used this technique to measure the m/z of single, 2.35 μm latex particles, which were large enough to be observed optically with illumination from a He-Ne laser (Philip, Gelbard, & Arnold, 1983). The absolute mass and charge of a trapped particle can be determined using a method they called "electron-stepping." With this method, the particles are exposed to UV radiation which caused electrons to be ejected; the m/z of the particle was then re-measured by adjusting the DC bias on the end caps. The process can be repeated several times to provide more m/z measurements and hence a more reliable mass determination. The mass resolving power achieved by the "electron-stepping" method is on the order of 10^2.

In 1995, Hars & Tass (1995) developed a third method to measure the m/z with QIT optical detection, which is more accurate than the two described above. When a charged particle oscillates in a QIT, as shown in Figure 2a, its trajectory projected

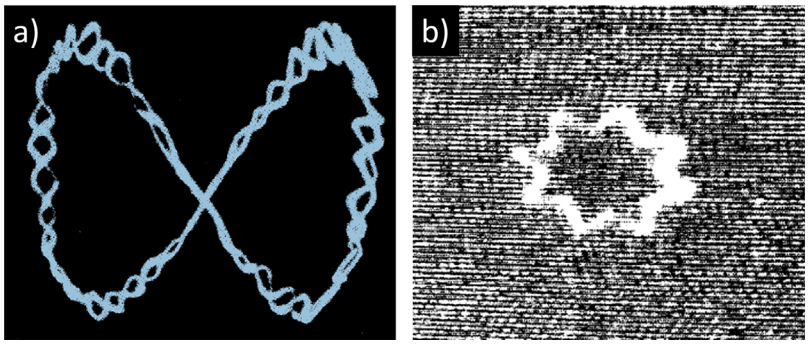

FIGURE 2. (**a**) Photograph of a single ion trajectory in a QIT observed through a hole in the ring electrode (perpendicular to the axis of the end caps). From Wuerker, Shelton, & Langmuir (1959). (**b**) Photograph of a single ion in a QIT observed along the axis of the end caps. From Hars & Tass (1995).

onto a perpendicular plane (i.e., the plane normal to the axis of the end caps) is elliptical with superimposed micromotions. If the ratio of the driving frequency (which causes the micromotions) to the secular frequency (the Lissajous motion) is an integer, then the elliptical trajectory appears as a stationary star pattern, as shown in Figure 2b. The m/z can be determined from the number of points on the star and the driving frequency and amplitude on the ring electrode. The absolute mass can be determined with the electron-stepping method described above, although here the drive frequency is changed to measure the new m/z. The resolving power was $\sim 10^3$ for μm-sized, $\sim 10^{12}$ Da polystyrene particles. The resolving power can be improved to the 10^4 range with an averaging peak-to-peak voltage detector to provide a more accurate measurement of the amplitude of the driving signal (Peng et al., 2005a).

Chang applied the same methodology in 2004 to measure the mass distribution of dry *Escherichia coli* cells ionized with MALDI (Peng et al., 2004). One-electron steps were induced with electron bombardment. The average mass of 60 cells was ~50 GDa. This measurement was the first time MS was applied to intact organisms above the 10 GDa mass range.

The Chang group also used the star pattern method with laser-induced acoustic desorption (LIAD). For LIAD, the sample was deposited directly on a silicon wafer, and a laser aimed at the back of the wafer caused acoustic, mechanical shaking forces that desorbed some of the sample. Some particles were apparently pre-charged and simply liberated from the substrate as ions (Peng et al., 2006). The masses of polystyrene spheres from NIST were measured. The measured masses were found to be within the expected range (Peng et al., 2005b). The technique was also applied to vaccinia virus (3.26×10^9 Da) and human red blood cells (RBCs). The substantial mass difference observed between normal RBCs (1.9×10^{13} Da) and anemic RBCs (1.3×10^{13} Da) (Peng et al., 2006) demonstrated the potential use of this technique for biomedical applications.

The three methods to measure the m/z in a QIT described above rely on the adjustment of settings until some characteristic of the particle motion is obtained. A more precise method of measuring the m/z is to maintain a constant frequency and voltage while the particle is illuminated with a laser (Schlemmer et al., 2001). The particle motion is on the order of the width of the beam, so the intensity of scattered light is modulated. Gerlich and co-workers replaced the QIT ring electrode with eight cylindrical rods to increase the acceptance angle of the scattered light onto the detector. In this trap, the AC voltage is applied to the end caps only. A fast Fourier transform (FFT) was used to extract all the frequencies of motion the particle undergoes, including motion in all three directions as well as combinations and higher harmonics. The resolving power of this method was 10^4 for 10 sec trapping of 500 nm SiO_2 particles, but it can be improved to better than 10^5 for trapping over an hour. This method is precise enough, and trapping times long enough, that adsorption and desorption rates of C_{60} from nanoparticles as well as binding energies could be measured over the course of weeks (Schlemmer et al., 2004). It was also used to study charging mechanisms of SiO_2 nanoparticles with soft X-rays (Grimm et al., 2006). Particles up to at least 50 μm have been trapped (Seo, Hong, & Boo, 2003).

The FFT measurement scheme has also been used with a cylindrical ion trap (Nie et al., 2006), which consists of a cylindrical electrode capped with two flat, electrically conductive glass plates. Scattered light can be detected through the transparent end caps. This design increases the detection efficiency of the scattered light. Viruses as small as the ~80 nm diameter adenovirus were measured.

The masses of nano- and micro-particles can be measured with very high precision while they are trapped in a QIT, but this technology is not suited for rapid analysis of many ions. In some cases, the trap has to be pumped out each time a new ion is introduced (Hars & Tass, 1995). Once an ion is injected, it can take tens of seconds to thermalize its motion before analysis is done (Schlemmer et al., 2001; Cai et al., 2002a). The electron-stepping method is critical for the mass measurement, but it is also time-consuming. Ionization by illumination or electron bombardment (Schlemmer et al., 2004) should be sufficiently inefficient that only one or a few charges are stripped at a time, so it typically takes several seconds for charge stripping to occur (Hars & Tass, 1995). Also, depending on how the m/z is measured, settings might have to be re-optimized to measure the new m/z each time a charge is stripped. Because each ion can, therefore, take minutes to analyze, measurement of a mass distribution of any unknown sample would be onerous. Mass distributions have typically been determined from measurements of tens of particles (Peng et al., 2004, 2005b). For more accurate estimates of mass heterogeneity, or for more heterogeneous samples, far more measurements would be needed. The long measurement time is not always a disadvantage. Because a single ion can be trapped almost indefinitely, its mass and charge can be tracked over time. Therefore, this technology is ideal for study of surface reaction kinetics, optical properties, or other properties of nano- or micro-particles in the gas phase. Some of these applications are discussed in part B of this section.

Chang and co-workers have developed a much faster method to measure the m/z of nanoparticles with a QIT (Cai et al., 2002a). However, with their method only a single m/z measurement can be made per ion, which precludes mass determination. Multiple polystyrene spheres of ~1 μm or diamond nanocrystals of ~100 nm generated by electrospray were trapped at the same time, and the end cap voltage was scanned. Each particle had a different m/z and would therefore be ejected through a hole drilled in the end cap at a different voltage. This axial instability mode is used for conventional QIT MS, in which an ion detector, usually MCPs, detects the ions as they are ejected. For single-particle detection, however, a continuous Ar ion laser illuminated the particles upon ejection, and the scattered light was detected. The timing of the scattered light was correlated with the ejection voltage to provide an m/z measurement with a resolving power of $\sim 10^2$ (Nie et al., 2008). Chang proposed the addition of a charge detector tube to measure the charge of each particle after its ejection, so that the m/z measurements could be converted to mass measurements; however, this addition has not been implemented.

B. Extension of the Mass Range to Smaller Particles

Single-molecule m/z measurements in a QIT have been performed for particles up to at least 50 μm (Seo, Hong, & Boo, 2003). However, determination of the m/z of a single particle with a QIT relies on optical detection. As stated

above, the light scattering intensity increases with diameter to the sixth power, which limits the technique to particles above ~50 nm diameter (Nie et al., 2006). Smaller particles can be detected this way if they are fluorescent.

Chang detected 27 nm, fluorescein-labeled polystyrene spheres in a QIT from their laser-induced fluorescence (LIF) (Cai et al., 2002b). Multiple particles were generated with MALDI and trapped at the same time. When a particle passed through an Ar ion laser focused into the center of the trap, detectable LIF was generated before photobleaching of the particle occurred. After the majority of particles had been bleached (which took only a few seconds), spikes of LIF were determined to be from an individual particle that passed through the laser's path. With many particles in the trap, and with only a short time before bleaching and consequent loss of signal, the *m/z* could not be determined.

To measure the *m/z*, Chang and co-workers developed a dual-QIT instrument (Cai, Peng, & Chang, 2003; Peng et al., 2003). The first QIT was used as the mass analyzer in axial instability mode, though here the frequency was scanned rather than the voltage. However, the interaction time between each ejected particle and a probe laser was too short to detect the LIF. The second QIT was used to collect the ejected particles, and continuous laser illumination of that trap provided LIF detection. This method was also used to obtain an *m/z* spectrum of fluorescently labeled, 150 kDa immunoglobulin G (IgG).

The disadvantage of non-specific fluorescent labeling, as in the two cases above, is that not every ion will have the same number of fluorophores. The resolution is insufficient to resolve each peak in the *m/z* spectrum, even for relatively small IgG. Because the absolute mass was not determined for each particle, it would be very difficult to determine an accurate mass of any unknown.

Intrinsically fluorescent particles do not have the limitation described above. Anderson and co-workers (Howder, Bell, & Anderson, 2014) measured the mass of single, 5 nm, ligand-coated CdSe/ZnS quantum dots (QDs) with a resolving power on the order of 10^6 in a split-ring QIT. They applied an AC waveform to an electrode just outside the trap. When this driving frequency was in resonance with the particle's secular frequency, the enlarged amplitude of the particle's motion removed it from the path of a probe laser focused in the center of the trap to result in a dip in LIF and consequent *m/z* determination. This approach is conceptually similar to Langmuir's original method to measure the *m/z* of a particle in a QIT (Wuerker, Shelton, & Langmuir, 1959), although the precision here is much better. These extremely precise measurements require a very slow scan of the driving frequency. If a faster scan speed is used, then resolving power is reduced (to the 10^2 range) (Howder, Bell, & Anderson, 2014), but changes in the mass of the particle can be tracked. For example, the mass of the 5 nm QDs slowly dropped over the course of about twelve hours, presumably from sublimation due to heating from the probe laser (Bell et al., 2014). Unlike the labeled particles studied by Chang, QDs can be tracked continuously for days without bleaching. Charge states were changed via collision with electrons, Ar^+, or Ar^* (electronically excited Ar) generated by the cold cathode gauge used to measure the argon pressure in the trap. Multiple *m/z* measurements provide the mass of each particle.

This technology has enabled the Anderson group to study a number of interesting features of single isolated QDs, such as fluorescence blinking (Bell et al., 2014) as well as intense brightening and drastic changes to emission spectra upon heating with a laser (Howder et al., 2014). They have also developed a method to use a trapped QD to probe the *m/z* of a co-trapped, dark particle of comparable size (Howder et al., 2015a). Figure 3 illustrates the concept. When the probe QD is alone in the trap (the black curve), there is a dip in LIF when the ion's secular frequency matches the scanned driving frequency (~22 kHz), as described above. When the dark particle is added (the red curve), its motion will also resonate when the driving frequency matches the particle's secular frequency (~5 kHz). Because the QD probe and the dark particle interact Coulombically, the dark particle's large-amplitude motion scatters the QD out of the laser beam to reduce the LIF signal and provide the *m/z* of the dark particle with a resolving power of $\sim 10^3$. The dip in LIF from the QD still appears at the same frequency, which indicates that the probe QD and the dark particle do not interfere with each other's secular frequencies even though they apparently interfere with each other's amplitudes. This method invites the study of particles too small to scatter sufficient light for optical detection but too large or heterogeneous for conventional MS: precisely the range of many important biological complexes, though the technology has not yet been applied to this type of problem.

Another way to analyze relatively small particles with a QIT is to heat them with a laser until thermal emission becomes detectable. Anderson and co-workers heated 20–50 nm carbon nanoparticles with several different lasers to several thousand Kelvin and studied sublimation and oxidation kinetics as well as optical properties of the nanoparticles (Howder et al., 2015b). Mass loss rates ranging from $\sim 10^1$ to 10^6 Da/min were tracked, so this technology is capable of probing a wide range of gas phase processes. The high temperatures attained in these studies are relevant for applications such as hypersonic flight and high-temperature combustion.

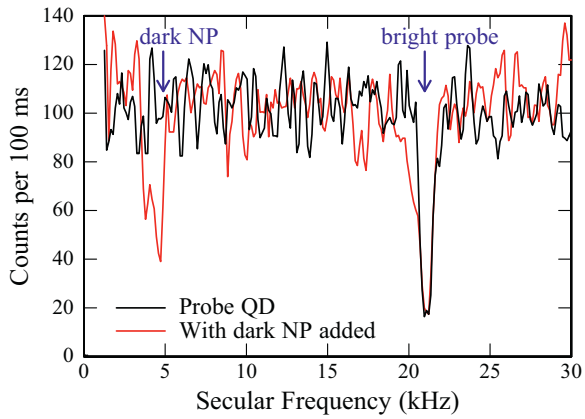

FIGURE 3. Plot of LIF detected as the secular frequency in a QIT is scanned. The black line shows a scan with only a bright probe (a QD) in the QIT. The LIF signal drops when the ion's secular frequency matches the driving frequency. The red line shows a scan with a dark particle added. A second drop in LIF is observed at the secular frequency of the dark ion. Adapted from Howder et al. (2015a).

IV. SINGLE-MOLECULE FOURIER TRANSFORM ION CYCLOTRON RESONANCE HERE

In the mid-1990s, Smith and co-workers used FTICR to perform single-molecule mass measurements. The approach is similar to single-molecule QIT in many ways. A trapped ion's *m*/*z* is measured with high precision; the charge state is stepped, and subsequent *m*/*z* measurements yield the mass (Smith et al., 1994; Bruce et al., 1994). With FTICR, single ions were isolated with stored-wave inverse Fourier transform (SWIFT), where all ions except for a narrow band of *m*/*z* values are excited and lost (Chen et al., 1987). After determination of the remaining ion's *m*/*z*, the charge was stepped by introduction of a gaseous reagent into the FTICR cell. The reagent is pumped out, and the *m*/*z* is re-measured. Several charge-stepping cycles were performed, and the mass determined. The resolving power was 10^4–10^5. Unlike QIT with optical detection, where the lower limit of detection is set by the intensity of the scattered or fluoresced light, the lower limit of detection in single-molecule FTICR is set by the smallest signal that can be measured on the detection plates; single proteins as small as 66 kDa BSA with 30 charges have been detected. BSA is much less massive than any single particle detected in a QIT. Single ions down to 17 kDa myoglobin with 20 charges have also been detected on the orbitrap (Makarov & Denisov, 2009), but only a single *m*/*z* measurement was done on each ion; therefore, mass was not determined.

As with single-molecule QIT experiments, single-molecule FTICR experiments are time-consuming. Up to a minute of collisional cooling and pumping-down (Bruce et al., 1994) was required for each ion before analysis even began, and determination of the mass with charge stepping is always laborious. Like single-molecule QIT, single-molecule FTICR is better-suited to monitoring a single ion over a long time period than to performing the large number of mass measurements needed to determine a mass distribution.

Smith and co-workers used FTICR to perform the first single-molecule mass measurement for a large biopolymer (Cheng et al., 1994). Masses were measured for 133 kDa BSA dimer ions. In this case, charge-stepping was accomplished via proton transfer to ammonia. Mass measurements were also performed for a 1.95 MDa plasmid (Cheng et al., 1996). Here, gaseous acetic acid was used to induce charge state steps through proton transfer; gas-phase adduction and elimination of acetic acid were also observed.

A second method to measure the mass of single molecules with FTICR involves direct charge detection. If the detection circuit capacitance and the radius of the cyclotron motion are known, then the total number of charges on an ion can be determined from the voltage drop across the detection circuit (Chen et al., 1994). For simplicity, the measurements were performed with only a single ion in the cell. The number of ions present can be determined from the frequency spectrum (except in the unlikely event that two large heterogeneous ions have exactly the same *m*/*z*). Multiplication of the *m*/*z* and charge of the ion yields the mass. However, the problem with this approach is that the radius of the cyclotron orbit is difficult to measure accurately. To estimate the radius, the ion cyclotron motion is excited, and the voltage drop across the detection circuit measured. The cyclotron motion is damped, and the process is repeated for higher and higher excitation amplitudes. The voltage drop across the detection circuit increases at each step because of the increased radius until, finally, the ion is excited to the point where it collides with an electrode and is lost. The voltage drop for the measurement just before the ion is lost is used for the charge measurement. For that measurement, it is assumed that the cyclotron radius is 95% of the cell radius. This approach has been applied to multi-MDa PEG ions (Chen et al., 1994), and a similar approach has been applied to 110 MDa T4 DNA ions (Chen et al., 1995b). To our knowledge, 110 MDa remains the record for largest mass successfully analyzed in FTICR. Unfortunately, the resolving power was only ∼10 because of significant uncertainty in the cyclotron radius and detector capacitance. Like charge stepping, direct charge detection in FTICR is a time-consuming process because multiple measurements are required.

V. CHARGE DETECTION MASS SPECTROMETRY

CDMS is a single-molecule technique where the *m*/*z* and the charge are both measured simultaneously. The concept is simple: an ion passes through a conducting cylinder and induces a charge on the cylinder. The induced charge is picked up by a charge-sensitive preamplifier. As long as the length to diameter ratio of the cylinder is greater than ∼4, the induced charge is equal in magnitude to the charge on the ion (Shockley, 1938; Weinheimer, 1988). This approach to measuring the charge is unlike the FTICR method mentioned above, where the induced charge is distributed between all the electrodes in the cell, not just the detection electrodes. Thus, knowledge of the ion trajectory is not required with CDMS. There are three modes of operation: single-pass measurements, a linear array of detector tubes, and a detector tube in an electrostatic ion trap so that the ion oscillates back and forth through the detector tube.

A. Single-Pass Measurements

The first CDMS measurements were performed in 1960 (although it was not called CDMS at the time) (Shelton, Hendricks, & Wuerker, 1960). Micrometer-sized iron spheres were accelerated through a 100 kV potential difference to ∼3 km/sec to study their impact craters on various surfaces. Because the induced charge only lasts as long as the particle is inside the detector tube, the velocity, and therefore the *m*/*z*, was determined from the width of the signal due to the induced charge or from the time between signals from consecutive detector cylinders. The charge was obtained from the amplitude of the signal. The particles were charged to $\sim 10^4$ e. The resolving power was only ∼5 because of the uncertainty in the charge measurement. In similar studies, a Van de Graaff generator was used to accelerate particles through a 6 MV potential difference (Keaton et al., 1990) in order to simulate cosmic dust impact on spacecraft. Charges as low as ∼2000 e were detected. Although this method is relatively imprecise, it allows the mass to be determined for ∼100 particles/sec (Stradling et al., 1993).

In 1995, Fuerstenau and Benner used electrospray to extend the technique into the MDa range (Fuerstenau & Benner, 1995) and opened the door to the future studies of biological species and nanoparticles. Their detector tube was connected to a JFET at the input of the charge-sensitive preamplifier. Because the signal was processed with a Gaussian differentiator, an ion entering the tube produced a pulse, and a pulse of opposite

polarity resulted when the ion exited. The polarity of the pulses depends on whether the ion is positively or negatively charged. The amplitudes of the pulses were used to determine the charge. The pulse area provides a better measure of the charge because the amplitude is affected by ion velocity. Nevertheless, the pulse amplitude has frequently been used for simplicity. Care was taken to minimize the capacitance of the detector, which minimized noise and maximized the response to a charge that passed through the cylinder. The charge measurement was calibrated by application of a test charge to the detector tube by means of a capacitor and a signal generator. With this setup, the RMS noise was 150 e. The limit of detection (the smallest charge that could be measured) was ~425 e. Masses were measured for DNA ions in the 3–30 MDa range.

A few years later, the RMS noise was reduced to 100 e, and the limit of detection was improved to ~300 e (Schultz, Hack, & Benner, 1998, 1999). The limit of detection effectively imposes a lower-mass limit; DNA masses could be measured down to ~1 MDa. Even with these improvements, the resolving power was still fairly poor, ~6. The resolving power was limited by the charge measurement, which was about an order of magnitude less precise than the *m/z* measurement. Benner and co-workers used the same methodology to measure the masses of intact viruses (Fuerstenau et al., 2001). The mass spectra measured for rice yellow mottle virus (6.6 MDa) and tobacco mosaic virus (40.5 MDa) are shown in Figure 4. Although the peak maxima are moderately accurate, the peaks were broad with large, high-mass tails. A lot of the breadth probably comes from the imprecision of the single-pass charge measurement used in this work.

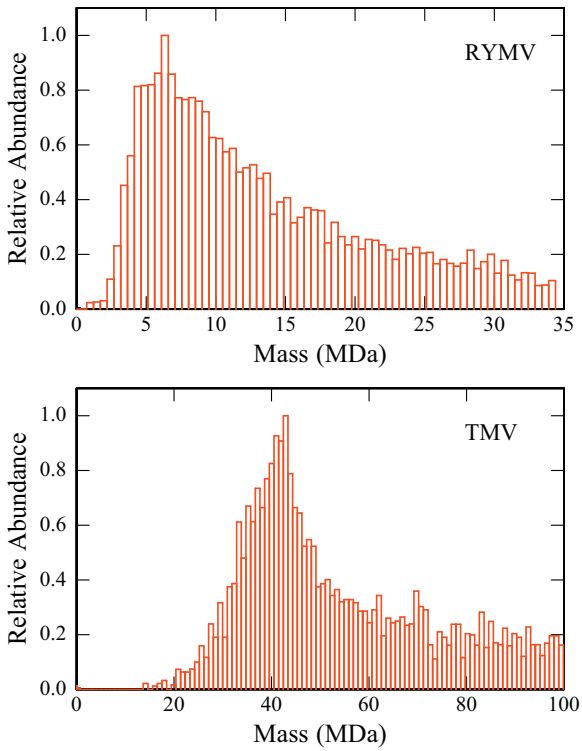

FIGURE 4. CDMS mass spectra measured for (**a**) rice yellow mottle virus (RYMV) and (**b**) tobacco mosaic virus (TMV). Adapted from Fuerstenau et al. (2001).

Antoine, Dugourd, and collaborators later applied this technology to synthetic polymers (Doussineau et al., 2011b), nanoparticles (Ouadah et al., 2013), composite nanoparticles (Doussineau et al., 2015a), self-assembled amphiphilic block copolymer micelles (Doussineau et al., 2012b, 2013), and vesicles (Warren et al., 2015) in the MDa-GDa range to study the charging mechanism in electrospray and polymeric nanoparticle mass distributions. Charging was consistent with the charge residue mechanism (Fernandez de la Mora, 2000), where the charged droplet evaporates from the analyte and deposits its leftover charge. Detection of >1000 ions/sec was achieved (Doussineau et al., 2011b). Figure 5 shows the mass distribution measured for composite nanoparticles that consisted of six polystyrene spheres (hexapods). The low-mass component is due to free polystyrene beads, whereas the higher mass component is due to hexapods. The resolving power in these measurements is limited by the uncertainty in the charge (~150 e RMSD). Because the hexapods carry on average ~5000 charges, the resolving power in this case is ~14 and the broad peak widths in Figure 5 are mainly due to the mass distribution of the nanoparticles. The charge and mass are determined for each ion in CDMS; thus, they can be correlated. The blue points in Figure 5 show a scatter plot of charge versus mass. The different slopes for the two components indicate different morphologies.

In the preceding work, the ion's *m/z* is determined from its TOF through the detector tube. To convert the TOF to the *m/z*, the ion's kinetic energy is required. The contribution to the kinetic energy from acceleration through a known potential difference in the instrument is easily determined, but the ions also pick up energy from the gas expansion into vacuum. The most common way to correct for the energy that the ions pick up from the expansion is to measure TOF with all electrodes grounded to determine the velocity from gas flow and subtract that velocity from the total velocity (Fuerstenau & Benner, 1995; Schultz, Hack, & Benner, 1998, 1999; Fuerstenau et al., 2001; Doussineau et al., 2011b, 2012b, 2013, 2015a; Ouadah et al., 2013; Warren et al., 2015). However, there is a broad distribution of velocities from the gas flow (Maze, Jones, & Jarrold, 2006), and it is better to account for the aerodynamic

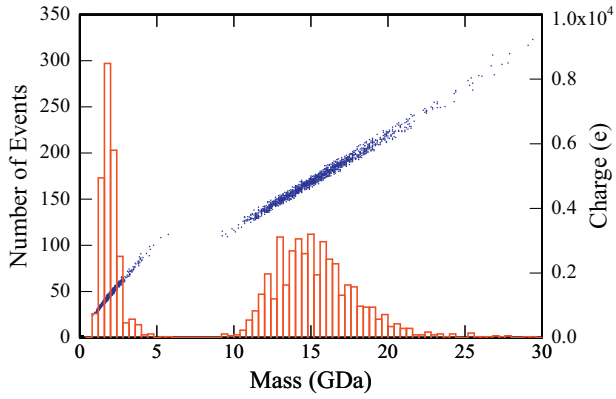

FIGURE 5. CDMS measurements for composite nanoparticles. The red histogram shows the mass distribution measured by CDMS for composite nanoparticles consisting of six polystyrene spheres (hexapods). The low mass component is due to free polystyrene beads. The blue points show the charges measured for each ion (right hand scale). Adapted from Doussineau et al. (2015a).

energy of each particle individually (Mabbett et al., 2007). One way to make this correction is to measure the velocity through a detector tube, accelerate the ion through a known potential difference, and re-measure the velocity with a second detector tube. The *m*/*z* is determined from the potential difference and the change in velocities. This approach has been used to study the aerodynamic break-up of electrosprayed water droplets as they travel through a differentially pumped interface (Zilch et al., 2009). A similar approach involves acceleration and then deceleration of the particles through a symmetric triangular potential ramp in between the two detector tubes (Zilch et al., 2008). In that case, the arrival time at the second tube is compared with the expected arrival time to calculate the *m*/*z*.

B. Linear Detector Array

The large uncertainty in the charge measurement and the high limit of detection with single-pass CDMS limits its applicability to highly charged objects. Signal averaging, either with a detector array or with an electrostatic ion trap, can overcome these limitations. A linear detector array consists of a series of cylinders that each ion passes through in turn. This approach was first used by Gamero-Castaño (2007). In principle, the uncertainty in the charge and the limit of detection should improve as the square root of the number of detectors. However, if all the cylinders are connected to the same amplifier, then the increased input capacitance limits the increase in performance. If a separate amplifier is used for each tube, then there is no limitation on the number of detector tubes that can be used, except for the effort required to maintain and calibrate all of the circuits. Usually a compromise is struck, where each amplifier is connected to several detector tubes. In Gamero-Castaño's original work, a linear array of six detector tubes was used. The first, third, and fifth detector tubes were connected to one amplifier, and the second, fourth, and sixth tubes were connected to another. The RMS noise was 100 e.

As noted above, an accurate determination of the *m*/*z* from the TOF requires knowledge of the ion energy. In subsequent work, Gamero-Castaño (2009) coupled a differential retarding potential energy analyzer to a linear detector array. Only ions within a narrow band of kinetic energies per charge were deflected by an appropriate angle to enter the array. This approach was used to study electrosprayed water nanodroplets, and it was found that 100–400 nm droplets were charged to between 50 and 100% of the Rayleigh limit. The method has also been used to study sputtering with electrosprayed droplets (Gamero-Castaño & Mahadevan, 2009).

The method to measure the *m*/*z* from two velocity measurements described above in the section on single-pass measurements (Mabbett et al., 2007) has been applied to a linear array of 22 detector tubes (Smith et al., 2011). The first 11 were all connected to one amplifier and held at one potential, and the next 11 were all connected to a second amplifier and held at another potential. A correlation analysis was used for each set to measure the charge and the velocity of electrosprayed polyethylene glycol ions. The velocity difference between the two sets was used to determine the energy and the *m*/*z*. With this improved methodology, the RMS charge uncertainty was reduced to 10 e. The limit of detection was improved to 100 e, which reduced the smallest mass that could be detected by CDMS to ~150 kDa.

Austin and co-workers recently showed that printed circuit boards (PCBs) could be used for CDMS (Barney, Daly, & Austin, 2013). An array of metal film strips on the PCBs were used as the electrodes. Two identical PCBs must be placed, face to face, one above the other; an ion that passes between them induces an image charge on each electrode. So far, this work has only been proof-of-principle; no mass measurements have been reported.

C. Electrostatic Ion Trap

A second way to reduce the uncertainty of the charge measurement is to trap individual ions in an electrostatic ion trap so that they oscillate back and forth through a central charge detector tube. Although this approach is much slower than single-pass detectors or linear arrays, it offers the lowest uncertainty in the charge measurement.

Benner first implemented CDMS with an electrostatic ion trap in 1997 (Benner, 1997). His trap, shown schematically in Figure 6, consisted of several flat, parallel electrodes on either side of a shielded detector tube. The electrodes have apertures so that ions can enter the trap. To initiate trapping, all front electrodes are grounded and the back electrodes are maintained at their trapping potentials. When an ion of sufficiently high charge is detected, the front electrodes are set to the same potentials as the back ones. The ion is trapped and oscillates back and forth through the detector tube. The mass of the ion was determined from the time-domain data for each cycle and averaged. Benner suggested that the charge measurement could be as precise as the RMS noise level at the detector (which was equivalent to 50 e). The noise should decrease as the reciprocal of the square root of the number of oscillations. In the best case, the ion underwent 450 cycles (~10 ms trapping time) to reduce the RMS noise to 2.3 e. However, the limit of detection was still relatively high (~250 e) because the increase of the potential on the front electrodes was triggered on a single pass.

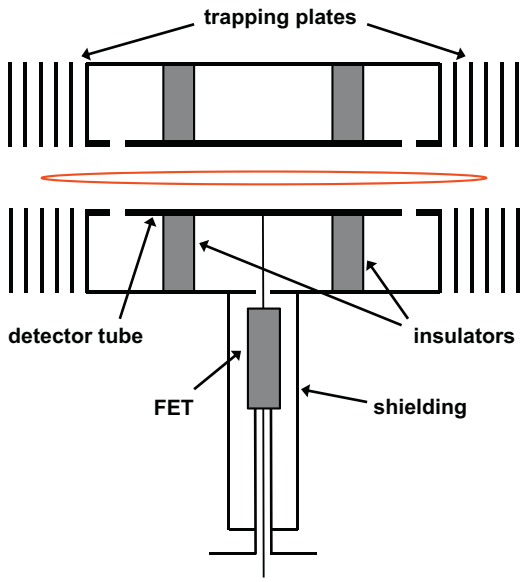

FIGURE 6. Schematic diagram of the electrostatic trap used by Benner to perform multiple measurements of the charge on a single ion. Adapted from Benner (1997).

A similar ion trap has been used by Antoine and co-workers to do tandem MS. They studied infrared multiphoton dissociation of MDa-range DNA (Doussineau et al., 2011a, 2012a, 2015b) and PEG (Antoine et al., 2013) ions. A single-pass charge detector tube preceded the trap and was used to trigger a trapping event for an ion with the appropriate mass and charge. Trapping times were improved to several tens of milliseconds. The ion was irradiated while it was trapped, and time-resolved analysis of the induced charge signal allowed calculation of dissociation rate constants and activation energies. This single-particle analysis illuminated several fragmentation pathways that could not have been detected from ensemble studies. An example of the signal recorded for multiphoton dissociation of a single λ-phage DNA ion stored in the trap under continuous irradiation is shown in Figure 7. The signal was processed with a Gaussian differentiator; for a cation a negative going pulse results when the ion enters the detector tube and a positive going pulse when it leaves. The amplitude of the leading pulse is used to determine the charge. In the example shown in Figure 7, the charge starts at 1700 e, and between 8 and 10 ms the signal gradually decreases as the ion dissociates and the fragments are ejected from the trap. An expanded view of the 8–10 ms time range is shown in the inset in Figure 7. The signal after 10 ms is due to noise.

Recent work by Jarrold and co-workers has reduced the uncertainty in the charge measurement and lowered the limit of detection in CDMS (Contino & Jarrold, 2013; Contino et al., 2013; Pierson et al., 2013, 2015; Keifer, Shinholt, & Jarrold, 2015). In the preceding work, the ion trap was closed when it was known that an ion was present (gated trapping). The presence of an ion was determined from a single-pass measurement leading to a high limit of detection. To reduce the limit of detection, Contino & Jarrold (2013) used continuous trapping, where the trap is continuously opened and closed for predetermined times. The resulting signals were analyzed off-line with FFTs. The ion's m/z was determined from the frequency of the fundamental, and the charge was determined from the magnitude. The limit of detection is much improved compared to gated trapping because the induced charge does not need to rise above the noise in the time domain. This improvement dramatically expands the range of species that can be studied. Ions with as few as six charges have been detected (Pierson et al., 2015). For light ions, the charge states are resolved in the m/z spectrum to allow a direct determination of the uncertainty in the charge measurement by comparing the measured charge to the charge assigned by the m/z. All previously reported uncertainties were inferred from simulations or noise levels.

For CDMS with a gated ion trap, it is necessary to restrict the signal to minimize the number of events where more than one ion is trapped. With continuous trapping, the trap might be empty, contain a single ion, or contain multiple ions. Trapping events that are empty or contain multiple ions are discarded during the data analysis. The maximum fraction of single-ion trapping events that can be realized is 37% (Pierson et al., 2015). If the average signal is increased beyond the optimum value, then the fraction of multiple-ion trapping events increases at the expense of single-ion events, and if it is decreased, then the fraction of empty trapping events increases.

Because the charge is quantized, it only needs to be measured with sufficient accuracy that the charge state can be assigned with a high degree of confidence. This level of accuracy requires an uncertainty (RMSD) in the charge measurement of better than ∼0.25 e. The main contribution to the uncertainty is electrical noise from the JFET at the input of the charge-sensitive preamplifier. Cryogenically cooling the JFET increases its transconductance, lowers thermal noise, and consequently improves the signal to noise ratio (Contino et al., 2013). The uncertainty in the charge measurement can be lowered further by trapping the ion for a longer time: the uncertainty decreases as the reciprocal of the square root of the trapping time. With a modified cone trap (Schmidt et al., 2001) optimized for long trapping times and operation at pressures in the ultra-high vacuum regime to minimize collisions with the background gas, trapping times of several seconds were obtained. With 3 s trapping, the uncertainty in the charge measurement was reduced to less than 0.20 e (RMSD) for pyruvate kinase (PK) multimers (Keifer, Shinholt, & Jarrold, 2015). Figure 8 shows the charge spectrum measured for PK ions trapped for 3 sec. The peaks in the spectrum are due to ions with a different number of charges. The group of peaks at ∼33 e is due to the PK tetramer,

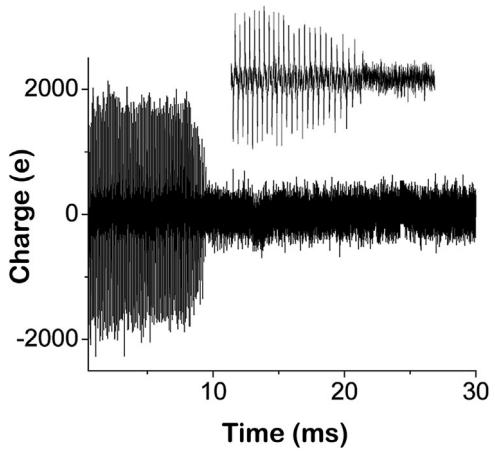

FIGURE 7. Signal recorded for a single λ-phage DNA ion stored in the ion trap under continuous irradiation with a CO_2 Laser (14.6 W/cm^2). The inset shows an expanded view of the signal between 8 and 10 ms. Adapted from Doussineau et al. (2012a).

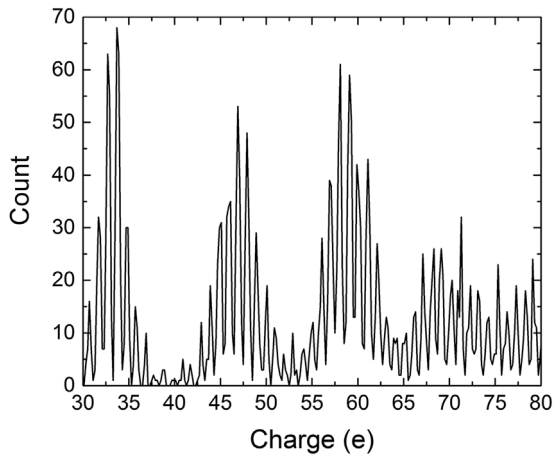

FIGURE 8. Charge spectrum measured with CDMS for pyruvate kinase ions trapped for 2991 ms. The bin width is 0.2 e, and the histogram contains 3125 ions. From Keifer, Shinholt, & Jarrold (2015).

the group at ∼45 e is due to the octamer, and group at ∼60 e is due to the dodecamer. When the charges are so well-resolved, it is possible to assign charge states. For ions with charges that are close to integral values, the assignment is unambiguous, but the assignment is ambiguous for ions with charges that lie near half-integral values. With an RMSD of 0.2 e, ions within one standard deviation of the mean (67% of the total) can be assigned to the correct charge state with an error rate of ∼1 in 15,000. With such a low error rate, the uncertainty in the mass measurement is almost entirely limited by the uncertainty in the m/z measurement.

The low uncertainty in the charge measurement described above was achieved for ions with masses less than 1.5 MDa and with fewer than 100 charges. As the mass of the ion increases, the m/z and charge both increase. A larger m/z leads to a lower oscillation frequency in the electrostatic trap. The noise is larger at lower frequency because of the $1/f$ contribution. This increase can be mitigated by raising the ion energy in the trap. For a fixed oscillation frequency, the uncertainty in the charge due to the noise is independent of the charge. Thus, if the uncertainty is 0.2 e at 60 e, then it will be 0.2 e at 600 e. However, as the contribution to the uncertainty from the noise is reduced by averaging, other contributions emerge. In particular, the magnitude of the signal in the FFT used to analyze the time domain signals depends on the duty cycle of the ions. The duty cycle depends slightly on the entrance conditions (the angle and radial offset of the ion's trajectory with respect to the trap axis) and the deviation of the ion energy from the design value. Ions that enter the trap off-axis undergo complex Lissajous-like trajectories. Keifer, Shinholt, & Jarrold (2015) showed that the uncertainty due to these factors can be minimized by summing the first and second harmonic in the FFT. However, the uncertainty in the charge measurement due to variations in the duty cycle scales with the charge; thus, this contribution becomes more important as the mass increases.

Charge-state resolution has been achieved for ions with fewer than 100 charges; however, the same precision has not yet been achieved for more highly charged ions. Also, the high-precision charge measurements were achieved mainly by extending the trapping time. Although the long trapping times demonstrate that high-precision charge measurements are feasible, they are not practical for routine applications. Finally, in cases where high-precision charge measurements have been performed, the mass resolution did not improve dramatically because the m/z resolution of the existing trap is relatively poor. The best mass resolving power that has been achieved to date is ∼100. Thus, although substantial improvements in CDMS performance metrics have been achieved in the last few years, a number of areas remain where further improvement is needed.

The improvements described above have opened the door to a number of important applications, particularly in the areas of virus assembly and virus analysis. For example, CDMS has been used to probe kinetically trapped intermediates in HBV assembly (Pierson et al., 2014) and non-icosahedral polymorphs in woodchuck hepatitis virus (WHV) (Pierson et al., 2016), helped to compare the temperature dependence of HBV and WHV assembly (Kukreja et al., 2014), and measured the distribution of scaffolding proteins in bacteriophage P22 (Keifer et al., 2014). Figure 9 shows a portion of the mass distribution measured for WHV assembly products. The main peak at just over 4.1 MDa is due to the $T=4$ capsid, an icosahedron that

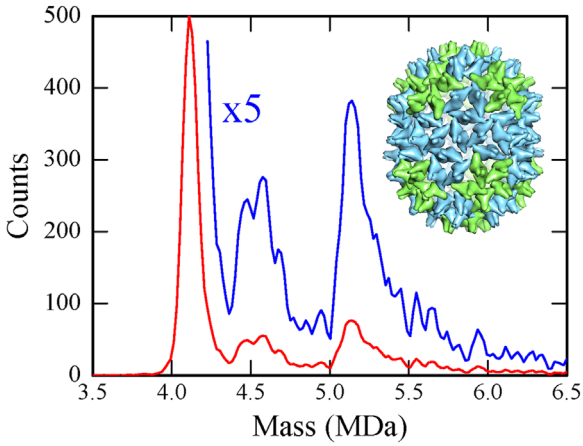

FIGURE 9. Mass distribution of WHV assembly products. The inset shows a possible structure for the oversized species with 150 dimers (∼5.1 MDa). Adapted from Pierson et al. (2016).

consists of 120 capsid protein dimers. As is evident from the mass distribution, there is a significant number of higher-mass species due to oversized capsids. The integrated intensity of the oversized capsids is roughly equal to the integrated intensity of the peak due to the $T=4$ capsid, thus around half of the assembly products are oversized. The prominent peak at just over 5.1 MDa is due to a species with 150 dimers. The prominence of this species suggests that it has a special structure. A plausible candidate is obtained by extending the $T=4$ capsid along its fivefold axis by adding a ring of hexamers. A model of this structure is shown in the inset in Figure 9.

VI. CHARGE DETECTION WITH A QUADRUPOLE ION TRAP

Another way to measure the m/z and charge of single particles is to trap some of them in a QIT and eject them, one at a time, onto a detector plate that acts as a Faraday cup. This approach was pioneered by Chen and co-workers in 2007 (Peng et al., 2007). The m/z is determined from the ring electrode frequency that ejects the ions. The detector plate is connected to a JFET at the input of an operational amplifier, and the amplitude of the signal due to the arriving ion provides a measure of the charge. However, because the RMS noise was ∼500 e this approach is only appropriate for very highly charged objects. The method has been called charge detection mass spectrometry, but we consider it to be a distinct from the CDMS methods described above because a single destructive measurement of the charge is performed.

Mass measurements have been performed for polystyrene microparticles and several types of intact cell in the 10^{12}–10^{15} Da range. The charged microparticles were generated by LIAD. However, because the LIAD generated microparticles usually had a charge less than 2000 e, a corona discharge was often used to increase the charge. Around two particles can be analyzed per second, which is much faster than with a QIT with optical detection. The resolving power, however, is only ∼7 because of the relatively low m/z resolution of a single-particle QIT in the axial instability mode and the poor precision of the charge measurement (Nie et al., 2007). Careful calibration of the QIT can improve the m/z resolving power to 100, although the

precision of the charge measurement is still the limiting factor (Nie et al., 2008).

The average masses of healthy and anemic human red blood cells were determined to differ by ∼40% with this technique, even though the heterogeneity of the cells and the poor mass precision make for only poorly resolved peaks in a mass distribution of a mixture of the cells. The kinetics of gold and polystyrene nanoparticles' endocytosis into cells was measured by observation of the shift in average mass of the cells after incubation of their solution with nanoparticles (Lin et al., 2010). A QIT with detector plate has also been used to characterize HPLC column-packing materials (Xiong et al., 2011).

Several approaches to simplify the technology have been explored. The scanned frequency applied to the ring electrode typically has a sinusoidal waveform, but rectangular and triangular waveforms provide comparable precision and are much easier to implement through digital electronics (Xiong et al., 2012). The whole device can be miniaturized and operated without a turbo pump by using the simpler cylindrical ion trap (CIT) with slightly reduced precision (Zhu et al., 2011). Finally, the LIAD ionization source traditionally used for this method requires a laser and is not very sensitive. A simpler aerodynamic desorption source liberates pre-charged particles from a substrate with a pulsed airflow, and was more sensitive than LIAD (Xiong et al., 2013). This source was used to measure the kinetics, pH dependence, and dissociation constant of protein adsorption to microparticles (Xiong et al., 2014).

VII. NANOMECHANICAL OSCILLATORS

The techniques discussed so far rely on one or several m/z measurements (and in some cases, also a charge measurement) to determine the mass. A wholly different approach is to measure the mass directly with a micro- or nanomechanical oscillator (Chen et al., 1995a). The resonant frequency of a mechanical oscillator depends on its mass. When a particle adsorbs on an oscillator its resonant frequency usually decreases. The frequency shift depends on the mass of the oscillator and the mass and position of the adsorbed particle; adsorption to a higher-amplitude location on the oscillator causes a larger shift (Dohn et al., 2005). Several ways to deal with the position issue have been devised, and will be described below. The smallest mass detected with this approach is ∼100 Da (Chaste et al., 2012). The resonator in that case was a short carbon nanotube held at 3×10^{-11} mbar.

Micromechanical oscillators were first used for single-particle analysis in 2001 when Ilic et al. (2001) measured the mass of individual *E. coli* cells. A 15–25 μm long, 5–10 μm wide, 320 nm thick silicon nitride cantilever was used. The method required coating the cantilever with *E. coli*-specific antibodies, measurement of its resonant frequency in air, immersion of the oscillator in a solution that contained *E. coli*, drying of the oscillator, measurement of the position of any adsorbed *E. coli* with scanning electron microscopy (SEM), and re-measurement of the resonant frequency. The average mass determined in this way was $\sim 4 \times 10^{11}$ Da. There are relatively large uncertainties in individual mass measurements due to uncertainties in the positions of the particles (from SEM) and in the resonant frequencies. The vibrational damping that occurs in air leads to a broad frequency bandwidth for the oscillator.

The approach employed in the preceding measurements is tedious and requires specific antibodies. Nevertheless, it demonstrated the feasibility of using a micromechanical oscillator for single-molecule mass analysis. Single-molecule mass measurements were also made for vaccinia virus (5.7 GDa) with the same approach (Gupta, Akin, & Bashir, 2004).

In related work, hollow microcantilevers have been used for single-molecule mass analysis of cells in solution (Burg et al., 2007; Godin et al., 2007). A buffer that contained cells flowed through the microcantelever, and, as a cell passed through, there was a transient resonant frequency shift that maximized when the particle reached the end of the cantilever. The technique measures the mass difference between the cell and the displaced buffer, and the densities of the buffer and cell are needed to determine the mass of the cell.

Performing the measurements in vacuum reduces the vibrational damping that occurs in air and substantially reduces the uncertainty in the frequency. In addition, it is desirable to avoid the use of SEM to locate the particles. One way around the position issue, introduced by Roukes and co-workers, is to perform an ensemble measurement, where hundreds or thousands of frequency shifts from single-particle adsorption events are detected and analyzed together (Naik et al., 2009). To demonstrate this approach 2.5 nm gold nanoparticles were electrosprayed and introduced through a differentially pumped interface. The detector stage was in a region held below 10^{-8} mbar, and the detector was cooled to 40 K to enhance physisorption (and to avoid the use of antibodies). A probability histogram of the frequency shifts was constructed, and with knowledge of the mass responsivity of the resonator and the shape of its fundamental bending mode, the average mass of the particles as well as the width of the distribution can be deduced. However, this method does not constitute a single-molecule mass measurement.

Single-molecule mass measurements can be made by measurement of the frequency shifts of two bending modes of an oscillator (Dohn et al., 2007; Schmid, Dohn, & Boisen, 2010). Dohn and co-workers showed that, with detailed knowledge of the shape of each bending mode, the two frequency shifts can be used to determine the mass and the position of the particle. In proof-of-principle studies, ∼μm-sized gold (Godin et al., 2007) or polystyrene beads (Naik et al., 2009) were manually placed on the oscillators.

The first attempt at single-molecule mass analysis with random adsorption was performed in 2012 by Roukes and co-workers (Hanay et al., 2012). In this work, the oscillator was a beam clamped at both ends and actuated electrostatically. Figure 10a shows a colorized electron micrograph of a device. The oscillator was cooled to 80 K, and the background pressure was $\sim 10^{-9}$ mbar. The resonant frequencies for the first two vibrational modes (which are shown in Fig. 10b) were tracked and used to determine the mass and position. Mass spectra were measured for 5 and 10 nm gold nanoparticles ionized with MALDI or electrospray. It is not possible to determine the precision of the mass measurements in this case because of the broad nanoparticle mass distribution. Figure 11 shows an electrospray mass spectrum of human IgM antibody subunits (∼190 kDa each) measured with the experimental configuration shown in Figure 10. The spectrum contains 73 ions binned into 100 kDa bins. The spectrum was interpreted as resulting from IgM aggregates with 3–12 IgM subunits with the maximum at

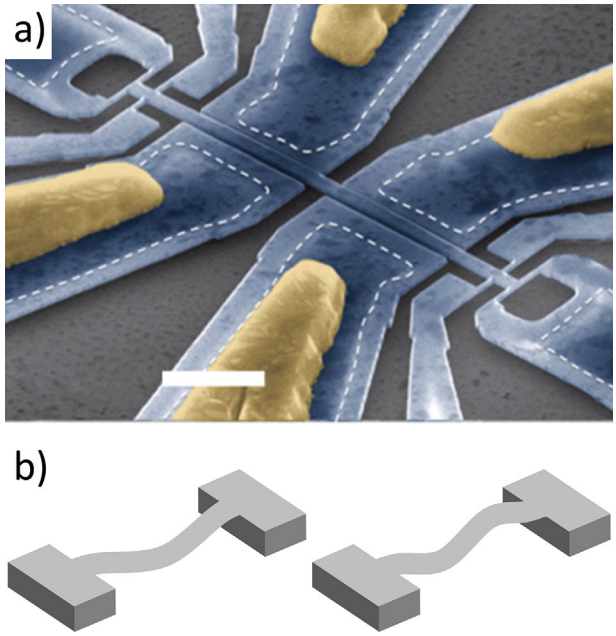

FIGURE 10. (**a**) Colorized electron micrograph of a nanomechanical oscillator. The white dotted line shows the boundaries of the region beneath the suspended device that anchors it to the substrate. The yellow regions represent Al/Si gate contacts. The narrow gauges near the ends of the beam become strained with the motion of the beam, thereby transducing mechanical motion into electric resistance. Scale bar: 2 μm. From Hanay et al. (2012). (**b**) The two vibrational modes of the oscillator used to deduce the mass.

5 subunits (at ∼950 kDa). Aggregates with even a few subunits are not resolved. Incomplete desolvation and chemical heterogeneity of IgM aggregates could contribute to the widths of the peaks (Lössl, Snijder, & Heck, 2014), but they are almost certainly not the main contributors. The relative precision might improve for more massive particles, because, theoretically, the uncertainty should be independent of the mass. However, this improvement in precision has not yet been demonstrated experimentally.

Measurement of the frequency shifts of more vibrational modes can in principle provide higher-order moments of the mass distribution (Hanay et al., 2015). For example, if the frequencies of five vibrational modes are monitored, then the mass, position (location of the particle's center of mass on the oscillator), length (standard deviation of the mass distribution), and asymmetry (skewness of the mass distribution) can be determined. At present, this kind of analysis neglects the effects of adsorbate stiffness, which are discussed below. In addition, because only longitudinal vibrational modes are monitored, information about the mass distribution is only available along one axis of the oscillator.

Like cryogenic detectors, nanomechanical oscillators can measure the masses of neutral particles (Sage et al., 2015). In recent work, tantalum nanoclusters in the MDa-range were generated with a sputtering gas aggregation source, which produced neutral and ionized clusters. Mass spectra measured with a nanomechanical oscillator and TOF m/z spectra were measured on the same instrument. The mass spectra measured with the nanomechanical oscillator looked similar whether or not ionized clusters were deflected away, which shows that the ionic and neutral clusters had similar mass distributions. In one example (see Fig. 12), the mass spectrum measured with the nanomechanical oscillator (labelled NOMS) and the TOF m/z spectrum measured with MCPs both showed a broad peak centered ∼2.4 MDa. In the TOF m/z spectrum, the peak occurs at 2.4 MDa and was attributed to ions with $z = 1$. There were also broad peaks in the m/z spectrum at lower m/z attributed to ions with $z = 2$ and $z = 3$. The 2.4 MDa peak in the TOFMS spectrum is ∼0.66 MDa wide (FWHM). This width is due to the broad cluster-size distribution. A 2.4 MDa tantalum cluster contains ∼13,000 atoms, and the individual cluster sizes are not

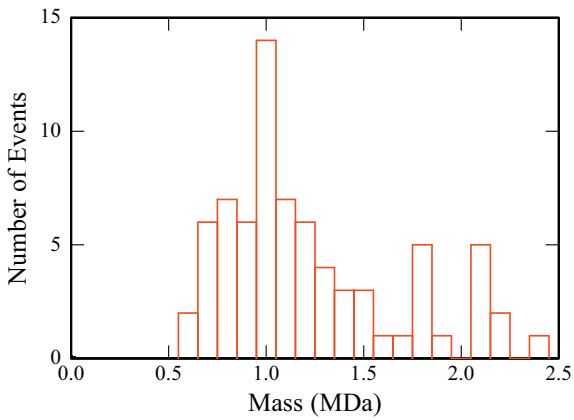

FIGURE 11. Mass spectrum measured for IgM using a nanomechanical oscillator. The spectrum contains 73 ions binned into 100 kDa bins. Adapted from Hanay et al. (2012).

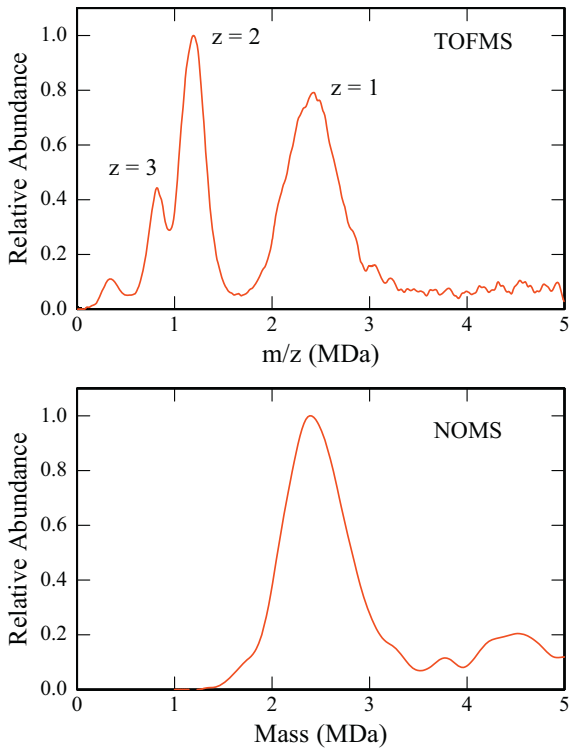

FIGURE 12. Mass spectra measured for tantalum clusters with TOF and MCP detectors (labelled TOFMS) and with a nanomechanical oscillator (labeled NOMS). Features attributed to $z = 1$, 2, and 3 are labelled in the TOFMS spectrum. Adapted from Sage et al. (2015).

TABLE 1. Comparison of the performance metrics for the different methods that have been used to perform single-molecule MS

Technique	Rate (particles/s)	Resolving Power	Mass Range (Da)	Limitations
Cryogenic Detector TOF	10-10^3	5-10^3	1-10^7	Poor energy resolution for charge determination
QIT Optical Detection				>50 nm or fluorescent
In-Trap Detection	10^{-4}-10^{-3}	10^2-10^6	10^5-10^{17}	
Axial Ejection	10^{-2}-10^{-1}	measures only *m*/*z*	10^5-10^{12}	
Single-Particle FTICR	10^{-3}-10^{-2}	10-10^5	10^5-10^8	>30 e
CDMS				
Single-pass	10^2-10^3	5-7	10^6-10^{13}	>300 e
Linear Array	10-10^2	~10	10^5-10^{12}	>100 e
Ion Trap	1-10	10-10^2	10^4-10^8	>6 e
QIT to Charge Detector	~2	~7	10^{12}-10^{15}	>10^3 e
Single-Particle NEMS	10^{-2}-2	~10	10^5-10^{14}	Spherical or must know stiffness

We only give metrics that have been demonstrated experimentally, not those that are theoretically possible.

resolved. The 2.4 MDa peak in the NOMS spectrum is 0.80 MDa wide (FWHM), which is slightly broader than the TOFMS peak. The difference between the peak widths can be used to obtain a rough estimate of the uncertainty in the nanomechanical mass measurements; the result is ~450 kDa (FWHM), so the resolving power at 2.4 MDa is estimated to be ~5.

A frequently overlooked complication with nanomechanical oscillators is that the stiffness and orientation of the adsorbate (if it is non-spherical) affects the resonant frequency (Gil-Santos et al., 2010; Ruz et al., 2014). The frequency can actually increase upon adsorption of a stiff particle. Therefore, mass and mechanical properties could both conceivably be measured. However, the ability to decouple all of the variables has not been demonstrated. The mechanical properties might contribute to the low precision of single-molecule mass measurements with nanomechanical oscillators. Also, the properties of the oscillator change as they accrete mass (Naik et al., 2009). This dependence provides an upper mass limit for single-molecule detection and the number of measurements that can be made with one oscillator.

The small size of the oscillator means that the vast majority of particles that enter the detector region bypass the detector. An even larger fraction of neutral particles will bypass the detector because they cannot be focused as easily as ions. The effective area of the detector is usually smaller than its physical size because particles that adsorb at a low-amplitude region of the oscillator will not produce a large enough frequency shift. Although an array of oscillators would increase the effective area, an array has not yet been demonstrated. Moreover, these devices are driven by phase-locked loops with a settling time on the order of several tens of milliseconds to seconds (Hanay et al., 2012; Sage et al., 2015). Consequently, the resonator frequencies must be measured for at least that amount of time for each adsorption event, which prevents rapid acquisition rates even if particles frequently strike the effective area of the detector.

VIII. CONCLUSIONS

Single-molecule techniques extend the mass range of MS to almost arbitrarily large values. They can also be used to obtain mass distributions for very heterogeneous samples and, in some cases, to do single-molecule kinetics experiments or to measure optical properties of single particles. These capabilities have allowed MS to provide valuable information for entirely new classes of object, such as nanoparticles and cells. Studies of the properties of individual ions can be performed to determine how they diverge from the ensemble average, along the lines of conventional single-molecule studies. A variety of methods have been used to perform single-molecule MS. We summarize their strengths and weaknesses in Table 1. We provide metrics for the measurement rate (the number of ions that can be measured per second), the accuracy of the mass measurements, and the mass range that has been accessed. We report metrics that have been demonstrated experimentally, not what are theoretically feasible. Sample consumption is not included in Table 1 because the amount needed depends strongly on the application. To measure a mass distribution containing 10^4 ions requires more sample than to measure the sublimation rate for a single nanoparticle. As a rule, single-molecule methods are usually less sensitive than conventional MS methods because the sample is used less efficiently. For some single molecule methods the detectors are small, so the probability of an ion striking the detector is low, and in others, the ions are only used for a fraction of the available time. On the other hand, single molecule methods can measure mass spectra for samples without the extensive purification steps needed to resolve charge states with conventional MS.

In general for single-molecule MS, there is a trade-off between precision and acquisition time, and this affects what kinds of applications are useful for each technique. Single-molecule FTICR and optical detection in a QIT can achieve mass precision on par with the best obtained with conventional MS, but it takes several minutes per particle to collisionally cool the ions after they have been injected, measure the *m*/*z*, shift the charge, re-measure the *m*/*z*, and sometimes repeat the shift and re-measure multiple times. For heterogeneous samples that might require thousands of mass measurements to obtain a reliable distribution, these techniques are impractical. On the other hand, these methods are well-suited to investigate the properties of individual ions, such as the measurement of the oxidation rates of nanoparticles with different gases, or conceivably for tandem MS on individual trapped ions. A QIT with optical detection is also ideally suited to measure optical properties of single particles.

TOF with a cryogenic detector and a QIT with a charge detector plate can be orders of magnitude faster than single-molecule FTICR and a QIT with optical detection, but they are relatively imprecise. The faster methods are more suitable for getting relatively rapid mass measurements of massive particles for applications where a precise mass measurement for each particle is not needed, such as water droplets or whole cells. TOF with cryogenic detectors can sometimes make moderately

precise mass measurements rather quickly; however, it is presently only useful for analytes with no more than a few charges. One benefit of TOF with cryogenic detectors is that neutral molecules can be detected, which has been useful for tandem MS experiments on small molecules.

CDMS is multifaceted in the trade-off between speed and precision. Single-pass and linear array CDMS are very fast, but the charge measurement is imprecise, which severely limits the mass precision. The low precision CDMS techniques are appropriate for the same types of applications as TOF with cryogenic detectors and QIT with a charge detector plate. CDMS with an ion trap has dramatically improved charge precision but requires longer acquisition times. Like single-molecule FTICR and QIT with optical detection, ion-trap CDMS can measure reaction kinetics of single particles in the gas phase, and it has been used for tandem MS experiments with infrared multiphoton dissociation. Ion-trap CDMS is faster than FTICR or QIT with optical detection, but it is not as precise, and trapping times are limited. It is precise enough in many cases, however, to measure stoichiometries of biological complexes such as virus capsids. All types of single-molecule MS are slower than conventional MS, but they can all extend to much higher masses (although this high-mass capability has not been demonstrated for cryogenic detectors).

The use of nanomechanical oscillators for single-molecule MS is the least-characterized of the techniques discussed here and requires a note on speed and precision. The measurement time for nanomechanical oscillators seems to be limited mostly by the low probability of particles striking the resonator, which is reduced to the nanoscale to enhance performance. The resonator itself does not need excessive time to respond to ion impact (several tens of milliseconds to seconds). Its relative mass precision has only been experimentally demonstrated for relatively small particles and is unimpressive. However, because its absolute precision is expected to be constant, relative precision might be substantially better for larger analytes. Until nanomechanical oscillators have become better characterized for single-molecule MS, it is difficult to predict what types of applications will be suitable.

Most types of single-molecule MS will continue to benefit from further technological advances. Cryogenic detectors can measure charge, but the signal is not proportional to the charge. This technology would benefit from improved energy resolution and elucidation of the relationship between signal amplitude and charge. Larger arrays of detectors would improve measurement rate. Large arrays do exist, but they have not yet been used for MS. The charge measurement for QIT with a charge detector plate is imprecise and limited by the noise level of the detector. Reduction of the noise would substantially improve the precision of that technique. The charge measurement in CDMS has been improved dramatically in recent years, but accurate charge measurements with CDMS require a single ion to be trapped for several seconds. Further reduction of the electrical noise would allow reduced acquisition times. Moreover, the precision of the m/z measurement in CDMS is relatively poor; it will need to be improved for the precision of CDMS to approach that of single-molecule FTICR and QITs with optical detection.

For nanomechanical oscillators, measurement speed currently seems to be limited by the rate that particles strike the detector. Arrays of oscillators would therefore improve the speed of these measurements. The published, experimental mass resolving power of these devices is unimpressive, but as discussed above, this should improve for more massive particles. Finally, nanomechanical oscillator measurements are complicated by the mechanical properties of the analyte particles. More improvements in data analysis, and measurements for more modes are required to account for those properties. If those improvements can be achieved it will be possible to measure mass and mechanical properties simultaneously, which would be a unique and exciting advance.

Single-molecule MS and conventional MS are complementary techniques. Many applications such as proteomics, glycomics, imaging, or any kind of high-throughput screening will almost certainly always be the domain of conventional MS because of the requirement for speed and the relatively small masses involved. On the other hand, the extension of the mass range with single-molecule MS has enabled the study of objects that have not been studied by MS before, including aerosols, liquid droplets, various inorganic particles, large synthetic polymers, cells, and organelles. In addition to information on the mass and heterogeneity, detailed study of fluorescence dynamics, adsorption rates, and more can all be performed at the single-molecule level. Small viruses are in the range of conventional and single-molecule MS, though heterogeneity can restrict the application of conventional MS. Larger viruses, like enveloped viruses, can only be studied with single-molecule MS.

ACKNOWLEDGMENT

We gratefully acknowledge the support of the National Science Foundation through grant CHE–1531823.

ABBREVIATIONS

BSA	bovine serum albumin
CAD	collisionally activated dissociation
CDMS	charge detection mass spectrometry
CIT	cylindrical ion trap
Cp149	149-residue assembly domain of capsid protein of hepatitis B virus
d	diameter
$E/\Delta E$	energy resolving power
ETD	electron-transfer dissociation
FFT	fast Fourier transform
FTICR	Fourier transform ion cyclotron resonance
FWHM	full width at half maximum
HBV	hepatitis B virus
LIAD	laser-induced acoustic desorption
LIF	laser-induced fluorescence
m/z	mass-to-charge ratio
$m/\Delta m$	mass resolving power
MALDI	matrix-assisted laser-desorption ionization
MCP	microchannel plate
MDa	megadalton
MS	mass spectrometry
NIS	normal insulator superconductor
PK	pyruvate kinase
PSD	post-source decay
QD	quantum dot
QIT	quadrupole ion trap
RBC	red blood cell

RMSD	root mean square deviation
SSLD	superconducting stripline detector
STJ	superconducting tunnel junction
SWIFT	stored-wave inverse Fourier transform
TOF	time-of-flight
WHV	woodchuck hepatitis virus
z	charge number

REFERENCES

Aksenov A, Bier M. 2008. The analysis of polystyrene and polystyrene aggregates into the mega dalton mass range by cryodetection MALDI TOF MS. J Am Soc Mass Spectrom 19:219–230.

Antoine R, Doussineau T, Dugourd P, Calvo F. 2013. Multiphoton dissociation of macromolecular ions at the single-molecule level. Phys Rev A 87:013435.

Barney BL, Daly RT, Austin DE. 2013. A multi-stage image charge detector made from printed circuit boards. Rev Sci Instrum 84:114101.

Bell DM, Howder CR, Johnson RC, Anderson SL. 2014. Single CdSe/ZnS nanocrystals in an ion trap: Charge and mass determination and photophysics evolution with changing mass, charge, and temperature. ACS Nano 8:2387–2398.

Benner WH. 1997. A gated electrostatic ion trap to repetitiously measure the charge and *m*/*z* of large electrospray ions. Anal Chem 69:4162–4168.

Benner WH, Horn DM, Jaklevic JM, Frank M, Mears C, Labov S, Barfknecht AT. 1997. Simultaneous measurement of flight time and energy of large matrix-assisted laser desorption ionization ions with a superconducting tunnel junction detector. J Am Soc Mass Spectrom 8:1094–1102.

Bereszczak J, Havlik M, Weiss V, Marchetti-Deschmann M, Duijn E, Watts N, Wingfield P, Allmaier G, Steven A, Heck AR. 2014. Sizing up large protein complexes by electrospray ionisation-based electrophoretic mobility and native mass spectrometry: Morphology selective binding of fabs to hepatitis B virus capsids. Anal Bioanal Chem 406:1437–1446.

Bruce JE, Cheng X, Bakhtiar R, Wu Q, Hofstadler SA, Anderson GA, Smith RD. 1994. Trapping, detection, and mass measurement of individual ions in a fourier transform ion cyclotron resonance mass spectrometer. J Am Chem Soc 116:7839–7847.

Burg TP, Godin M, Knudsen SM, Shen W, Carlson G, Foster JS, Babcock K, Manalis SR. 2007. Weighing of biomolecules, single cells and single nanoparticles in fluid. Nature 446:1066–1069.

Cai Y, Peng WP, Kuo SJ, Lee YT, Chang HC. 2002a. Single-particle mass spectrometry of polystyrene microspheres and diamond nanocrystals. Anal Chem 74:232–238.

Cai Y, Peng WP, Kuo SJ, Sabu S, Han CC, Chang HC. 2002b. Optical detection and charge-state analysis of MALDI-generated particles with molecular masses larger than 5 MDa. Anal Chem 74:4434–4440.

Cai Y, Peng WP, Chang HC. 2003. Ion trap mass spectrometry of fluorescently labeled Nanoparticles. Anal Chem 75:1805–1811.

Casaburi A, Zen N, Suzuki K, Ejrnaes M, Pagano S, Cristiano R, Ohkubo M. 2009. Subnanosecond time response of large-area superconducting stripline detectors for keV molecular ions. Appl Phys Lett 94:212502.

Casaburi A, Esposito E, Ejrnaes M, Suzuki K, Ohkubo M, Pagano S, Cristiano R. 2012. A 2×2 mm 2 superconducting strip-line detector for high-performance time-of-flight mass spectrometry. Supercond Sci Technol 25:115004.

Chang H-C. 2009. Ultrahigh-mass mass spectrometry of single biomolecules and bioparticles. Annu Rev Anal Chem 2:169–185.

Chaste J, Eichler A, Moser J, Ceballos G, Rurali R, Bachtold A. 2012. A nanomechanical mass sensor with yoctogram resolution. Nat Nanotechnol 7:301–304.

Chen L, Wang TCL, Ricca TL, Marshall AG. 1987. Phase-modulated stored waveform inverse fourier transform excitation for trapped ion mass spectrometry. Anal Chem 59:449–454.

Chen R, Wu Q, Mitchell DW, Hofstadler SA, Rockwood AL, Smith RD. 1994. Direct charge number and molecular weight determination of large individual ions by electrospray ionization fourier transform ion cyclotron resonance mass spectrometry. Anal Chem 66:3964–3969.

Chen GY, Thundat T, Wachter EA, Warmack RJ. 1995a. Adsorption-induced surface stress and its effects on resonance frequency of microcantilevers. J Appl Phys 77:3618–3622.

Chen R, Cheng X, Mitchell DW, Hofstadler SA, Wu Q, Rockwood AL, Sherman MG, Smith RD. 1995b. Trapping, detection, and mass determination of coliphage T4 DNA ions by electrospray ionization fourier transform ion cyclotron resonance mass spectrometry. Anal Chem 67:1159–1163.

Cheng X, Bakhtiar R, Van Orden S, Smith RD. 1994. Charge-state shifting of individual multiply-charged ions of bovine albumin dimer and molecular weight determination using an individual-ion approach. Anal Chem 66:2084–2087.

Cheng X, Camp DG, Wu Q, Bakhtiar R, Springer DL, Morris BJ, Bruce JE, Anderson GA, Edmonds CG, Smith RD. 1996. Molecular weight determination of plasmid DNA using electrospray ionization mass spectrometry. Nucleic Acids Res 24:2183–2189.

Chowdhury SK, Katta V, Chait BT. 1990. Probing conformational changes in proteins by mass spectrometry. J Am Chem Soc 112:9012–9013.

Contino NC, Jarrold MF. 2013. Charge detection mass spectrometry for single ions with a limit of detection of 30 charges. Int J Mass Spectrom 345–347:153–159.

Contino NC, Pierson EE, Keifer DZ, Jarrold MF. 2013. Charge detection mass spectrometry with resolved charge states. J Am Soc Mass Spectrom 24:101–108.

Dohn S, Sandberg R, Svendsen W, Boisen A. 2005. Enhanced functionality of cantilever based mass sensors using higher modes. Appl Phys Lett 86:233501.

Dohn S, Svendsen W, Boisen A, Hansen O. 2007. Mass and position determination of attached particles on cantilever based mass sensors. Rev Sci Instrum 78:103303.

Doussineau T, Bao CY, Clavier C, Dagany X, Kerleroux M, Antoine R, Dugourd P. 2011a. Infrared multiphoton dissociation tandem charge detection-mass spectrometry of single megadalton electrosprayed ions. Rev Sci Instrum 82:084104–084108.

Doussineau T, Kerleroux M, Dagany X, Clavier C, Barbaire M, Maurelli J, Antoine R, Dugourd P. 2011b. Charging megadalton poly(ethylene oxide)s by electrospray ionization. A charge detection mass spectrometry study. Rapid Commun Mass Spectrom 25:617–623.

Doussineau T, Antoine R, Santacreu M, Dugourd P. 2012a. Pushing the limit of infrared multiphoton dissociation to megadalton-size DNA ions. J Phys Chem Lett 3:2141–2145.

Doussineau T, Bao CY, Antoine R, Dugourd P, Zhang W, D'Agosto F, Charleux B. 2012b. Direct molar mass determination of self-assembled amphiphilic block copolymer nanoobjects using electrospray-charge detection mass spectrometry. ACS Macro Lett 1:414–417.

Doussineau T, Santacreu M, Antoine R, Dugourd P, Zhang W, Chaduc I, Lansalot M, D'Agosto F, Charleux B. 2013. The charging of micellar nanoparticles in electrospray ionization. Chem Phys Chem 14:603–609.

Doussineau T, Désert A, Lambert O, Taveau J-C, Lansalot M, Dugourd P, Bourgeat-Lami E, Ravaine S, Duguet E, Antoine R. 2015a. Charge detection mass spectrometry for the characterization of mass and surface area of composite nanoparticles. J Phys Chem C 119:10844–10849.

Doussineau T, Paletto P, Dugourd P, Antoine R. 2015b. Multiphoton dissociation of electrosprayed megadalton-sized DNA ions in a charge-detection mass spectrometer. J Am Soc Mass Spectrom 26:7–13.

Dubois F, Knochenmuss R, Zenobi R. 1999. Optimization of an ion-to-photon detector for large molecules in mass spectrometry. Rapid Commun Mass Spectrom 13:1958–1967.

Dyachenko A, Wang GB, Belov M, Makarov A, de Jong RN, van den Bremer ETJ, Parren PWHI, Heck AJR. 2015. Tandem native mass-spectrometry on antibody-drug conjugates and submillion da antibody-antigen protein assemblies on an orbitrap EMR equipped with a high-mass quadrupole mass selector. Anal Chem 87:6095–6102.

Fernandez de la Mora J. 2000. Electrospray ionization of large multiply charged species proceeds via Dole's charged residue mechanism. Anal Chim Acta 406:93–104.

Frank M, Mears CA, Labov SE, Benner WH, Horn D, Jaklevic JM, Barfknecht AT. 1996. High-efficiency detection of 66 000 Da protein molecules using a cryogenic detector in a matrix-assisted laser desorption/ionization time-of-flight mass spectrometer. Rapid Commun Mass Spectrom 10:1946–1950.

Frank M, Labov SE, Westmacott G, Benner WH. 1999. Energy-sensitive cryogenic detectors for high-mass biomolecule mass spectrometry. Mass Spectrom Rev 18:155–186.

Fraser GW. 2002. The ion detection efficiency of microchannel plates (MCPs). Int J Mass Spectrom 215:13–30.

Friedrich S, Harris J, Warburton WK, Carpenter MH, Hall JA, Cantor R. 2014. 112-pixel arrays of high-efficiency STJ X-ray detectors. J Low Temp Phys 176:553–559.

Fuerstenau SD, Benner WH, Thomas JJ, Brugidou C, Bothner B, Siuzdak G. 2001. Mass spectrometry of an intact virus. Angew Chem 113:559–562.

Fuerstenau SD, Benner WH. 1995. Molecular weight determination of megadalton DNA electrospray ions using charge detection time-of-flight mass spectrometry. Rapid Commun Mass Spectrom 9:1528–1538.

Gamero-Castaño M, Mahadevan M. 2009. Sputtering of silicon by a beamlet of electrosprayed nanodroplets. Appl Surf Sci 255:8556–8561.

Gamero-Castaño M. 2007. Induction charge detector with multiple sensing stages. Rev Sci Instrum 78:043301–043307.

Gamero-Castaño M. 2009. Retarding potential and induction charge detectors in tandem for measuring the charge and mass of nanodroplets. Rev Sci Instrum 80:053301–053304.

Ganem B, Li YT, Henion JD. 1991. Detection of noncovalent receptor-ligand complexes by mass spectrometry. J Am Chem Soc 113:6294–6296.

Gilmore IS, Seah MP. 2000. Ion detection efficiency in SIMS:: Dependencies on energy, mass and composition for microchannel plates used in mass spectrometry. Int J Mass Spectrom 202:217–229.

Gil-Santos E, Ramos D, Martinez J, Fernandez-Regulez M, Garcia R, San Paulo A, Calleja M, Tamayo J. 2010. Nanomechanical mass sensing and stiffness spectrometry based on two-dimensional vibrations of resonant nanowires. Nat Nanotechnol 5:641–645.

Godin M, Bryan AK, Burg TP, Babcock K, Manalis SR. 2007. Measuring Mass, Density, and size of particles and cells using a suspended microchannel resonator. Appl Phys Lett 91:123121.

Grimm M, Langer B, Schlemmer S, Lischke T, Becker U, Widdra W, Gerlich D, Flesch R, Rühl E. 2006. Charging mechanisms of trapped element-selectively excited nanoparticles exposed to soft x rays. Phys Rev Lett 96:066801.

Gupta A, Akin D, Bashir R. 2004. Single virus particle mass detection using microresonators with nanoscale thickness. Appl Phys Lett 84:1976–1978.

Hanay MS, Kelber S, Naik AK, Chi D, Hentz S, Bullard EC, Colinet E, Duraffourg L, Roukes ML. 2012. Single-protein nanomechanical mass spectrometry in real time. Nat Nanotechnol 7:602–608.

Hanay MS, Kelber SI, O'Connell CD, Mulvaney P, Sader JE, Roukes ML. 2015. Inertial Imaging with nanomechanical systems. Nat Nano 10:339–344.

Hars G, Tass Z. 1995. Application of quadrupole ion trap for the accurate mass determination of submicron size charged particles. J Appl Phys 77:4245–4250.

Hilton GC, Martinis JM, Wollman DA, Irwin KD, Dulcie LL, Gerber D, Gillevet PM, Twerenbold D. 1998. Impact energy measurement in time-of-flight mass spectrometry with cryogenic microcalorimeters. Nature 391:672–675.

Howder CR, Bell DM, Anderson SL. 2014. Optically detected, single nanoparticle mass spectrometer with pre-filtered electrospray nanoparticle source. Rev Sci Instrum 85:014104.

Howder CR, Long BA, Bell DM, Furakawa KH, Johnson RC, Fang Z, Anderson SL. 2014. Photoluminescence of charged CdSe/ZnS quantum dots in the gas phase: Effects of charge and heating on absorption and emission probabilities. ACS Nano 8:12534–12548.

Howder CR, Long BA, Bell DM, Anderson SL. 2015a. Thermally brightened CdSe/ZnS quantum dots as noncontact probes for surface chemistry studies of dark nanoparticles trapped in the gas phase. J Phys Chem C 119:14561–14570.

Howder CR, Long BA, Gerlich D, Alley RN, Anderson SL. 2015b. Single nanoparticle mass spectrometry as a high temperature kinetics tool: Sublimation, oxidation, and emission spectra of hot carbon nanoparticles. J Phys Chem A 119:12538–12550.

Hu Q, Cooks RG, Noll RJ. 2007. Phase-enhanced selective ion ejection in an Orbitrap mass spectrometer. J Am Soc Mass Spectrom 18:980–983.

Ilic B, Czaplewski D, Zalalutdinov M, Craighead HG, Neuzil P, Campagnolo C, Batt C. 2001. Single cell detection with micromechanical oscillators. J Vac Sci Technol B 19:2825–2828.

Keaton PW, Idzorek GC, Rowton LJ, Sr., Stradling GL, Bergeson SD, Collopy MT, Curling HL, Jr., McColl DB, Smith JD. 1990. A hypervelocity—Microparticle—Impacts laboratory with 0-km/s projectiles. Int J Impact Eng 10:295–308.

Keifer DZ, Pierson EE, Hogan JA, Bedwell GJ, Prevelige PE, Jarrold MF. 2014. Charge Detection mass spectrometry of bacteriophage P22 procapsid distributions above 20 MDa. Rapid Commun Mass Spectrom 28:483–488.

Keifer DZ, Shinholt DL, Jarrold MF. 2015. Charge detection mass spectrometry with almost perfect charge accuracy. Anal Chem 87:10330–10337.

Koji S, Shigehito M, Shigetomo S, Zhen W, Masataka O. 2008. Time resolution improvement of superconducting NbN stripline detectors for time-of-flight mass spectrometry. Appl Phys Express 1:031702.

Kukreja AA, Wang JC-Y, Pierson E, Keifer DZ, Selzer L, Tan Z, Dragnea B, Jarrold MF, Zlotnick A. 2014. Structurally similar woodchuck and human hepadnavirus core proteins have distinctly different temperature dependences of assembly. J Virol 88:14105–14115.

Li M-H, Tsai S-T, Chen C-H, Chen CW, Lee YT, Wang Y-S. 2007. Bipolar ion detector based on sequential conversion reactions. Anal Chem 79:1277–1282.

Lin H-C, Lin H-H, Kao C-Y, Yu AL, Peng W-P, Chen C-H. 2010. Quantitative measurement of nano-/microparticle endocytosis by cell mass spectrometry. Angew Chem Int Ed 49:3460–3464.

Loo JA. 1997. Studying noncovalent protein complexes by electrospray ionization mass spectrometry. Mass Spectrom Rev 16:1–23.

Lössl P, Snijder J, Heck AR. 2014. Boundaries of mass resolution in native mass spectrometry. J Am Soc Mass Spectrom 25:906–917.

Mabbett SR, Zilch LW, Maze JT, Smith JW, Jarrold MF. 2007. Pulsed acceleration charge detection mass spectrometry: Application to weighing electrosprayed droplets. Anal Chem 79:8431–8439.

Makarov A, Denisov E. 2009. Dynamics of ions of intact proteins in the Orbitrap mass analyzer. J Am Soc Mass Spectrom 20:1486–1495.

Marshall AG, Hendrickson CL, Jackson GS. 1998. Fourier transform ion cyclotron resonance mass spectrometry: A primer. Mass Spectrom Rev 17:1–35.

Maze JT, Jones TC, Jarrold MF. 2006. Negative droplets from positive electrospray. J Phys Chem A 110:12607–12612.

Naik AK, Hanay MS, Hiebert WK, Feng XL, Roukes ML. 2009. Towards single-molecule nanomechanical mass spectrometry. Nat Nanotechnol 4:445–450.

Nie Z, Cui F, Chu M, Chen C-H, Chang H-C, Cai Y. 2008. Calibration of a frequency-scan quadrupole ion trap mass spectrometer for microparticle mass analysis. Int J Mass Spectrom 270:8–15.

Nie Z, Cui F, Tzeng Y-K, Chang H-C, Chu M, Lin H-C, Chen C-H, Lin H-H, Yu AL. 2007. High-speed mass analysis of whole erythrocytes by charge-detection quadrupole ion trap mass spectrometry. Anal Chem 79:7401–7407.

Nie Z, Tzeng Y-K, Chang H-C, Chiu C-C, Chang C-Y, Chang C-M, Tao M-H. 2006. Microscopy-based mass measurement of a single whole virus in a cylindrical ion trap. Angew Chem Int Ed 45:8131–8134.

Novotný O, Allgeier S, Enss C, Fleischmann A, Gamer L, Hengstler D, Kempf S, Krantz C, Pabinger A, Pies C, Savin DW, Schwalm D, Wolf A. 2015. Cryogenic micro-calorimeters for mass spectrometric identification of neutral molecules and molecular fragments. J Appl Phys 118:104503.

Ohkubo M, Shigeri Y, Kinumi T, Saito N, Ukibe M, Chen YE, Kushino A, Kurokawa A, Sato H, Ichimura S. 2006. Fragmentation analysis by superconducting ion detectors in matrix-assisted laser desorption/ionization (MALDI). Nucl Instrum Methods Phys Res, Sect A 559:779–781.

Ohkubo M, Shiki S, Ukibe M, Tomita S, Hayakawa S. 2011. Direct mass analysis of neutral molecules by superconductivity. Int J Mass Spectrom 299:94–101.

Ouadah N, Doussineau T, Hamada T, Dugourd P, Bordes C, Antoine R. 2013. Correlation between the charge of polymer particles in solution and in the gas phase investigated by zeta-potential measurements and electrospray ionization mass spectrometry. Langmuir 29:14074–14081.

Park J, Qin H, Scalf M, Hilger RT, Westphall MS, Smith LM, Blick RH. 2011. A mechanical nanomembrane detector for time-of-flight mass spectrometry. Nano Lett 11:3681–3684.

Park J, Aksamija Z, Shin H-C, Kim H, Blick RH. 2013. Phonon-assisted field emission in silicon nanomembranes for time-of-flight mass spectrometry of proteins. Nano Lett 13:2698–2703.

Peng W-P, Cai Y, Lee YT, Chang HC. 2003. Laser-induced fluorescence/ion trap as a detector for mass spectrometric analysis of nanoparticles. Int J Mass Spectrom 229:67–76.

Peng W-P, Yang Y-C, Kang M-W, Lee YT, Chang H-C. 2004. Measuring masses of single bacterial whole cells with a quadrupole ion trap. J Am Chem Soc 126:11766–11767.

Peng W-P, Lee YT, Ting JW, Chang H-C. 2005a. Averaging peak-to-peak voltage detector for absolute mass determination of single particles with quadrupole ion traps. Rev Sci Instrum 76:023108.

Peng W-P, Yang Y-C, Lin C-W, Chang H-C. 2005b. Molar mass and molar mass distribution of polystyrene particle size standards. Anal Chem 77:7084–7089.

Peng W-P, Yang Y-C, Kang M-W, Tzeng Y-K, Nie Z, Chang H-C, Chang W, Chen C-H. 2006. Laser-induced acoustic desorption mass spectrometry of single bioparticles. Angew Chem Int Ed 45:1423–1426.

Peng W-P, Lin H-C, Lin H-H, Chu M, Yu AL, Chang H-C, Chen C-H. 2007. Charge-monitoring laser-induced acoustic desorption mass spectrometry for cell and microparticle mass distribution measurement. Angew Chem Int Ed 46:3865–3869.

Peng W-P, Chou S-W, Patil AA. 2014. Measuring masses of large biomolecules and bioparticles using mass spectrometric techniques. Analyst 139:3507–3523.

Philip MA, Gelbard F, Arnold S. 1983. An absolute method for aerosol particle mass and charge measurement. J Colloid Interface Sci 91:507–515.

Pierson EE, Keifer DZ, Contino NC, Jarrold MF. 2013. Probing higher order multimers of pyruvate kinase with charge detection mass spectrometry. Int J Mass Spectrom 337:50–56.

Pierson EE, Keifer DZ, Selzer L, Lee LS, Contino NC, Wang JCY, Zlotnick A, Jarrold MF. 2014. Detection of late intermediates in virus capsid assembly by charge detection mass spectrometry. J Am Chem Soc 136:3536–3541.

Pierson E, Contino N, Keifer D, Jarrold M. 2015. Charge detection mass spectrometry for single ions with an uncertainty in the charge measurement of 0.65 e. J Am Soc Mass Spectrom 26:1213–1220.

Pierson EE, Keifer DZ, Kukreja AA, Wang JCY, Zlotnick A, Jarrold MF. 2016. Charge detection mass spectrometry identifies preferred non-icosahedral polymorphs in the self-assembly of woodchuck hepatitis virus capsids. J Mol Biol 428:292–300.

Plath LD, Ozdemir A, Aksenov AA, Bier ME. 2015. Determination of iron content and dispersity of intact ferritin by superconducting tunnel junction cryodetection mass spectrometry. Anal Chem 87:8985–8993.

Rabin MW, Hilton GC, Martinis JM. 2001a. Application of ion-impact energy measurement to electrospray ionization mass spectrometry of proteins and protein mixtures. J Am Soc Mass Spectrom 12:826–831.

Rabin MW, Hilton GC, Martinis JM. 2001b. Application of microcalorimeter energy measurement to biopolymer mass spectrometry. IEEE Trans Appl Supercond 11:242–247.

Rose RJ, Damoc E, Denisov E, Makarov A, Heck AJR. 2012. High-sensitivity Orbitrap mass analysis of intact macromolecular assemblies. Nat Methods 9:1084–1086.

Ruz JJ, Tamayo J, Pini V, Kosaka PM, Calleja M. 2014. Physics of nanomechanical spectrometry of viruses. Sci Rep 4:6051.

Sage E, Brenac A, Alava T, Morel R, Dupré C, Hanay MS, Roukes ML, Duraffourg L, Masselon C, Hentz S. 2015. Neutral particle mass spectrometry with nanomechanical systems. Nat Commun 6:6482.

Schlemmer S, Illemann J, Wellert S, Gerlich D. 2001. Nondestructive high-resolution and absolute mass determination of single charged particles in a three-dimensional quadrupole trap. J Appl Phys 90:5410–5418.

Schlemmer S, Wellert S, Windisch F, Grimm M, Barth S, Gerlich D. 2004. Interaction of electrons and molecules with a single trapped nanoparticle. Appl Phys A 78:629–636.

Schmid S, Dohn S, Boisen A. 2010. Real-time particle mass spectrometry based on resonant micro strings. Sensors 10:8092.

Schmidt HT, Cederquist H, Jensen J, Fardi A. 2001. Conetrap: A compact electrostatic ion trap. Nucl Instrum Methods Phys Res, Sect B 173:523–527.

Schultz JC, Hack CA, Benner WH. 1998. Mass determination of megadalton-DNA electrospray ions using charge detection mass spectrometry. J Am Soc Mass Spectrom 9:305–313.

Schultz JC, Hack CA, Benner WH. 1999. Polymerase chain reaction products analyzed by charge detection mass spectrometry. Rapid Commun Mass Spectrom 13:15–20.

Seo SC, Hong SK, Boo DW. 2003. Single nanoparticle ion trap (SNIT): A novel tool for studying *in-situ* dynamics of single nanoparticles. Bull Korean Chem Soc 24:552–554.

Shelton H, Hendricks JCD, Wuerker RF. 1960. Electrostatic acceleration of microparticles to hypervelocities. J Appl Phys 31:1243–1246.

Shiki S, Ukibe M, Maeda R, Ohkubo M, Sato Y, Tomita S. 2008. Energy resolution improvement of superconducting tunnel junction particle detectors with infrared-blocking filters. Nucl Instrum Methods Phys Res, Sect A 595:391–394.

Shockley W. 1938. Currents to conductors induced by a moving point charge. J Appl Phys 9:635–636.

Smith RD, Cheng X, Bruce JE, Hofstadler SA, Anderson GA. 1994. Trapping, detection and reaction of very large single molecular ions by mass spectrometry. Nature 369:137–139.

Smith JW, Siegel EE, Maze JT, Jarrold MF. 2011. Image charge detection mass spectrometry: Pushing the envelope with sensitivity and accuracy. Anal Chem 83:950–956.

Snijder J, Heck AJR. 2014. Analytical approaches for size and mass analysis of large protein assemblies. Annu Rev Anal Chem 7:43–64.

Snijder J, Rose RJ, Veesler D, Johnson JE, Heck AJR. 2013. Studying 18 MDa virus assemblies with native mass spectrometry. Angew Chem Int Ed 52:4020–4023.

Snijder J, van de Waterbeemd M, Damoc E, Denisov E, Grinfeld D, Bennett A, Agbandje-McKenna M, Makarov A, Heck AJR. 2014. Defining the

stoichiometry and cargo load of viral and bacterial nanoparticles by Orbitrap mass spectrometry. J Am Chem Soc 136:7295–7299.

Spengler B, Kirsch D, Kaufmann R, Karas M, Hillenkamp F, Giessmann U. 1990. The Detection of large molecules in matrix-assisted UV-laser desorption. Rapid Commun Mass Spectrom 4:301–305.

Stockley PG, Rolfsson O, Thompson GS, Basnak G, Francese S, Stonehouse NJ, Homans SW, Ashcroft AE. 2007. A simple, RNA-mediated allosteric switch controls the pathway to formation of a T = 3 viral capsid. J Mol Biol 369:541–552.

Stradling GL, Idzorek GC, Shafer BP, Curling HL, Jr., Collopy MT, Blossom AAH, Fuerstenau S. 1993. Ultra-high velocity impacts: Cratering studies of microscopic impacts from 3 km/s to 30 km/s. Int J Impact Eng 14:719–727.

Suzuki K, Miki S, Wang Z, Kobayashi Y, Shiki S, Ohkubo M. 2008. Superconducting NbN thin-film nanowire detectors for time-of-flight mass spectrometry. J Low Temp Phys 151:766–770.

Tito MA, Tars K, Valegard K, Hajdu J, Robinson CV. 2000. Electrospray time-of-flight mass spectrometry of the intact MS2 virus capsid. J Am Chem Soc 122:3550–3551.

Twerenbold D, Vuilleumier JL, Gerber D, Tadsen A, van den Brandt B, Gillevet PM. 1996. Detection of single macromolecules using a cryogenic particle detector coupled to a biopolymer mass spectrometer. Appl Phys Lett 68:3503–3505.

Twerenbold D. 1996. Biopolymer mass spectrometer with cryogenic particle detectors. Nucl Instrum Methods Phys Res, Sect A 370:253–255.

Uetrecht C, Versluis C, Watts NR, Roos WH, Wuite GJL, Wingfield PT, Steven AC, Heck AJR. 2008a. High-resolution mass spectrometry of viral assemblies: Molecular composition and stability of dimorphic hepatitis B virus capsids. Proc Natl Acad Sci 105:9216–9220.

Uetrecht C, Versluis C, Watts NR, Wingfield PT, Steven AC, Heck AJR. 2008b. Stability and shape of hepatitis B virus capsids in vacuo. Angew Chem Int Ed 47:6247–6251.

Uetrecht C, Watts NR, Stahl SJ, Wingfield PT, Steven AC, Heck AJR. 2010. Subunit exchange rates in hepatitis B virus capsids are geometry- and temperature-dependent. Phys Chem Chem Phys 12:13368–13371.

van den Heuvel RHH, Heck AJR. 2004. Native protein mass Spectrometry: From intact oligomers to functional machineries. Curr Opin Chem Biol 8:519–526.

Warren NJ, Mykhaylyk OO, Ryan AJ, Williams M, Doussineau T, Dugourd P, Antoine R, Portale G, Armes SP. 2015. Testing the vesicular morphology to destruction: Birth and death of diblock copolymer vesicles prepared via polymerization-induced self-assembly. J Am Chem Soc 137:1929–1937.

Weidmann S, Zenobi R. 2014. High-mass MALDI-MS using ion conversion dynode detectors: Influence of the conversion voltage on sensitivity and spectral quality. J Am Soc Mass Spectrom 25:950–954.

Weinheimer AJ. 1988. The charge induced on a conducting cylinder by a point charge and its application to the measurement of charge on precipitation. J Atmos Oceanic Technol 5:298–304.

Wenzel RJ, Matter U, Schultheis L, Zenobi R. 2005. Analysis of megadalton ions using cryodetection MALDI time-of-flight mass spectrometry. Anal Chem 77:4329–4337.

Westmacott G, Frank M, Labov SE, Benner WH. 2000. Using a superconducting tunnel junction detector to measure the secondary electron emission efficiency for a microchannel plate detector bombarded by large molecular ions. Rapid Commun Mass Spectrom 14:1854–1861.

Wong SF, Meng CK, Fenn JB. 1988. Multiple charging in electrospray ionization of poly(ethylene glycols). J Phys Chem 92:546–550.

Wuerker RF, Shelton H, Langmuir RV. 1959. Electrodynamic containment of charged particles. J Appl Phys 30:342–349.

Xiong C, Zhou X, Chen R, Zhang Y, Peng W-P, Nie Z, Chang H-C, Liu H, Chen Y. 2011. Characterization of column packing materials in high-performance liquid chromatography by charge-detection quadrupole ion trap mass spectrometry. Anal Chem 83:5400–5406.

Xiong C, Xu G, Zhou X, Wang J, Tang Y, Chen R, Peng W-P, Chang H-C, Nie Z. 2012. The development of charge detection-quadrupole ion trap mass spectrometry driven by rectangular and triangular waves. Analyst 137:1199–1204.

Xiong C, Zhou X, Wang J, Zhang N, Peng W-P, Chang H-C, Nie Z. 2013. Ambient aerodynamic desorption/ionization method for microparticle mass measurement. Anal Chem 85:4370–4375.

Xiong C, Zhou X, Zhang N, Zhan L, Chen S, Wang J, Peng W-P, Chang H-C, Nie Z. 2014. Quantitative assessment of protein adsorption on microparticles with particle mass spectrometry. Anal Chem 86:3876–3881.

Zen N, Suzuki K, Shiki S, Ukibe M, Casaburi A, Ejrnaes M, Cristiano R, Ohkubo M. 2012. Operation of superconducting nano-stripline detector (SSLD) mounted on cryogen-free cryostat. Phys Procedia 27:356–359.

Zhou M, Robinson CV. 2010. When proteomics meets structural biology. Trends Biochem Sci 35:522–529.

Zhu Z, Xiong C, Xu G, Liu H, Zhou X, Chen R, Peng W-P, Nie Z. 2011. Characterization of bioparticles using a miniature cylindrical ion trap mass spectrometer operated at rough vacuum. Analyst 136:1305–1309.

Zilch LW, Maze JT, Smith JW, Ewing GE, Jarrold MF. 2008. Charge separation in the aerodynamic breakup of micrometer-sized water droplets. J Phys Chem A 112:13352–13363.

Zilch LW, Maze JT, Smith JW, Jarrold MF. 2009. Freezing, fragmentation, and charge separation in sonic sprayed water droplets. Int J Mass Spectrom 283:191–199.